Computer-Aided Craniomaxillofacial Surgery Planning

CHENG, YUAN

NATIONAL UNIVERSITY OF SINGAPORE

2011

Abstract

Many patients suffer from skull deformity which may greatly affect the their life qualities and even threaten their lives. To restore the normal appearance of the skull, the craniomaxillofacial (CMF) surgery is performed. This surgery is very complex and careful pre-operative planning is needed. In the planning, the repositioning of the bone fragments to restore the deformed skull is very important.

There are two related problems in CMF surgery planning, namely restoration and reconstruction. Restoration seeks to restore the deformed model back to its normal state by repositioning the bones in the deformed model. It directly gives the surgery plan. Reconstruction, on the other hand, derives an estimate of the normal model from the deformed model by shape similarity. To use reconstructed model for surgery planning, the surgeon needs to manually work out how to reposition the patient's bones to match the reference as given by the reconstructed model. At present, existing automatic restoration methods are unreliable.

Many computer-aided systems have been developed for CMF planning. Reactive systems are real-time systems that attempt to simulate the reactions of the body in response to user inputs. They are more suitable for surgery training than surgery planning. Predictive systems attempt to accurately predict surgical results of complex surgical procedures based on predefined or user-specified surgical requirements. They are suitable for planning complex CMF surgery. Some systems generate reconstructed model. Several systems can generate surgery plan for mandible restoration.

This thesis proposal developed a computer-aided procedure for assisting a surgeon in deriving a CMF surgery plan. This procedure, first segments the patient's bone fragments from medical images and constructs his/her deformed model from the segmentation result, then acquires surgical requirements from the surgeon through a graphical user interface, and finally restores the patient's skull model based on the requirements.

Contents

List of Figures . . . iii

List of Tables . . . v

1 Introduction **1**

1.1 Motivation . . . 1

1.2 Research Goal . . . 5

1.3 Organization of Thesis Proposal . . . 6

2 Background **9**

2.1 Skull . . . 9

2.2 Important Planes of the Skull . . . 10

2.3 Skull Deformities . . . 11

2.4 CMF Surgery . . . 13

3 Related Work **19**

3.1 Restoration and Reconstruction . . . 19

3.1.1 Manual Manipulation . . . 19

3.1.2 Symmetry-Based Reconstruction . . . 21

3.1.3 Geometric Reconstruction . . . 22

3.1.4 Statistical Reconstruction . . . 23

3.1.5 Fracture Surface Matching . . . 25

3.2 Computer-Aided Surgery Planning Systems . . . 26

3.2.1 Reactive Systems . . . 27

3.2.2 Predictive Systems 28
3.3 Summary 29

4 Proposed Thesis Project **32**
4.1 CMF Surgery Planning Procedure 32
4.1.1 Segmentation and Construction of 3D Deformed Model 33
4.1.2 Identification of Midline Landmarks and Fixed Bone Fragments . . . 35
4.2 Restoration of Deformed Model 38
4.2.1 Inputs 38
4.2.2 Principles 38
4.2.3 Restoration Algorithm 46
4.3 Research Schedule 48

5 Preliminary Work **50**
5.1 FICP Registration 50
5.2 FP, MSP and Midline Landmark Identification 52

6 Conclusion **56**

References **58**

List of Figures

1.1 Congenital cleft palate . . . 2

1.2 Congenital skull asymmetry . . . 2

1.3 Skull deformity due to accident . . . 3

1.4 A satisfactory CMF surgery result . . . 7

1.5 An unsatisfactory CMF surgery result . . . 8

2.1 Skull bones . . . 10

2.2 Frankfurt plane, mid-sagittal plane, and craniometric landmarks . . . 12

2.3 Skull deformities . . . 14

2.4 CMF surgery on deformed skull . . . 15

2.5 Result of CMF surgery . . . 17

2.6 Bone fragment not moved in surgery . . . 18

3.1 Manual restoration . . . 20

3.2 Symmetry-based reconstruction . . . 21

3.3 Semi-automatic methods for identifying the MSP . . . 22

3.4 Geometric-based reconstruction . . . 23

3.5 Statistical mandible shape model . . . 24

3.6 Statistical reconstruction of mandible . . . 24

3.7 Fracture surface matching method . . . 25

3.8 Fracture surface matching method on multiple fracture case . . . 25

3.9 Reactive system that simulates bone removal operation . . . 27

4.1 CT images of a patient's skull 33

4.2 Threshold segmentation 34

4.3 Snake segmentation 35

4.4 Segmentation and 3D deformed model construction result 36

4.5 Graphical user interface for identification of midline landmarks and fixed bone fragments 37

4.6 No collision principle 39

4.7 Difference between normal skull models and a reference model 41

4.8 Distribution of mean difference 41

4.9 Mean local variation of difference 42

4.10 Mean variation of difference distribution 43

4.11 Normality principle 44

4.12 Ordering principle 45

5.1 Comparison of FICP and ICP on registering similar models 51

5.2 Comparison of FICP and ICP on registering models with large variance . . 52

5.3 Identified MSP and FP 55

List of Tables

3.1 Comparison of restoration & reconstruction methods 31

5.1 Comparison of mean error 54

Chapter 1

Introduction

1.1 Motivation

Many patients suffer from skull deformity congenitally or in accidents. Worldwide, one in 700 children is born with cleft palate [Wro10], i.e., opening of the roof of the mouth (Figure 1.1), and one in $5,600$ children is born with facial asymmetry [Lit10] (Figure 1.2). In addition, many patients suffer from head and facial injuries that typically result in deformities such as fracture of the skull and jaws. For example, In North America, every year, around 1.58 million people suffer from head and facial injuries, due to traffic accidents (Figure 1.3), work accidents, home accidents, sports injuries, and violence [Wik12, GTH*03]. In Singapore, there are 10 public hospitals and 13 private hospitals. National University Hospital (NUH) along receives about 250-350 patients with skull fracture every year.

Skull deformities may lead to inaesthetic facial appearance as well as incomplete functionalities because the muscles and skins attached to a deformed skull are also deformed [LP98]. For example, jaw deformity (Figure 1.2) may affect the movement of the jaws, leading to chewing problem. Orbit (eye socket) deformity (Figure 1.3 (d)) may affect the ability of the skull to support the eye ball, which may lead to impaired vision. Nasal deformity may choke the airway and cause breathing difficulty. These problems greatly affect the patients' quality of life and even threaten their lives.

To correct skull deformities and restore the normal appearance of the skull, craniomaxillofacial (CMF) surgery is performed. CMF surgery involves complex operations on the jaws and skull [LP98, Ltd06]. As an example, let us consider a patient whose skull was severely deformed in an accident (Figure 1.5). The patient's frontal skull was broken into fragments and depressed inward. The right cheek bone was broken into several small fragments and displaced backward. The right eye socket was also broken leaving the eye ball unsupported, and the lower jaw was broken into two parts. To treat this patient, the

(a) (b)

Figure 1.1: Congenital cleft palate [Wik10]. (a) A six-month old child with cleft palate. (b) One month after surgery.

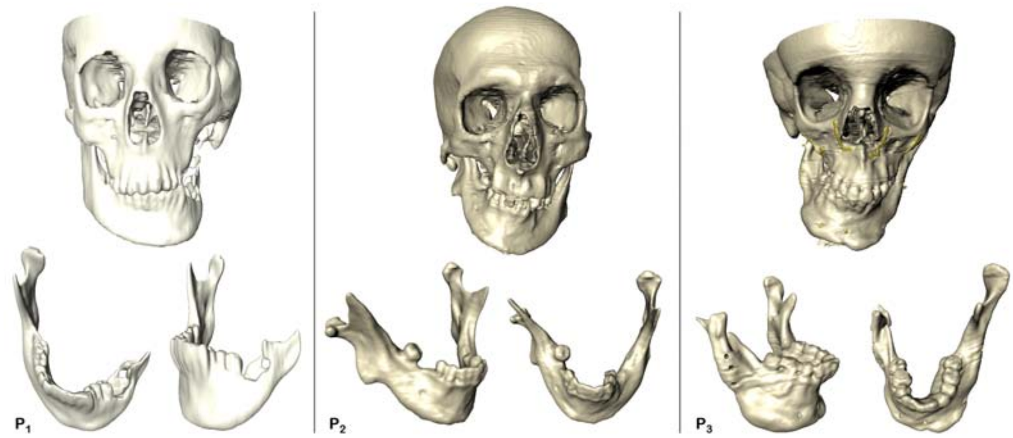

Figure 1.2: Congenital skull asymmetry [ZLES05]. (Top) The skulls are severely deformed congenitally. Large amount of left-right asymmetry exists in these skulls. (Bottom) Various views of the deformed jaws.

CMF surgeon in NUH pulled back the usable fragments of the frontal bone and held them in correct positions using metal meshes, put back the cheek bone and held it in the correct position using metal plates, inserted metal meshes into the eye socket floor to provide support for the eye ball, and used metal plates to hold the two lower jaw fragments in correct position to allow healing (Figure 1.4).

As can be seen, the whole CMF procedure is very difficult and complex. In addition to the procedural complexity, difficulties of performing such a surgery also result from the variation of patients' anatomical structures. Therefore, careful pre-operative planning of CMF surgery is important.

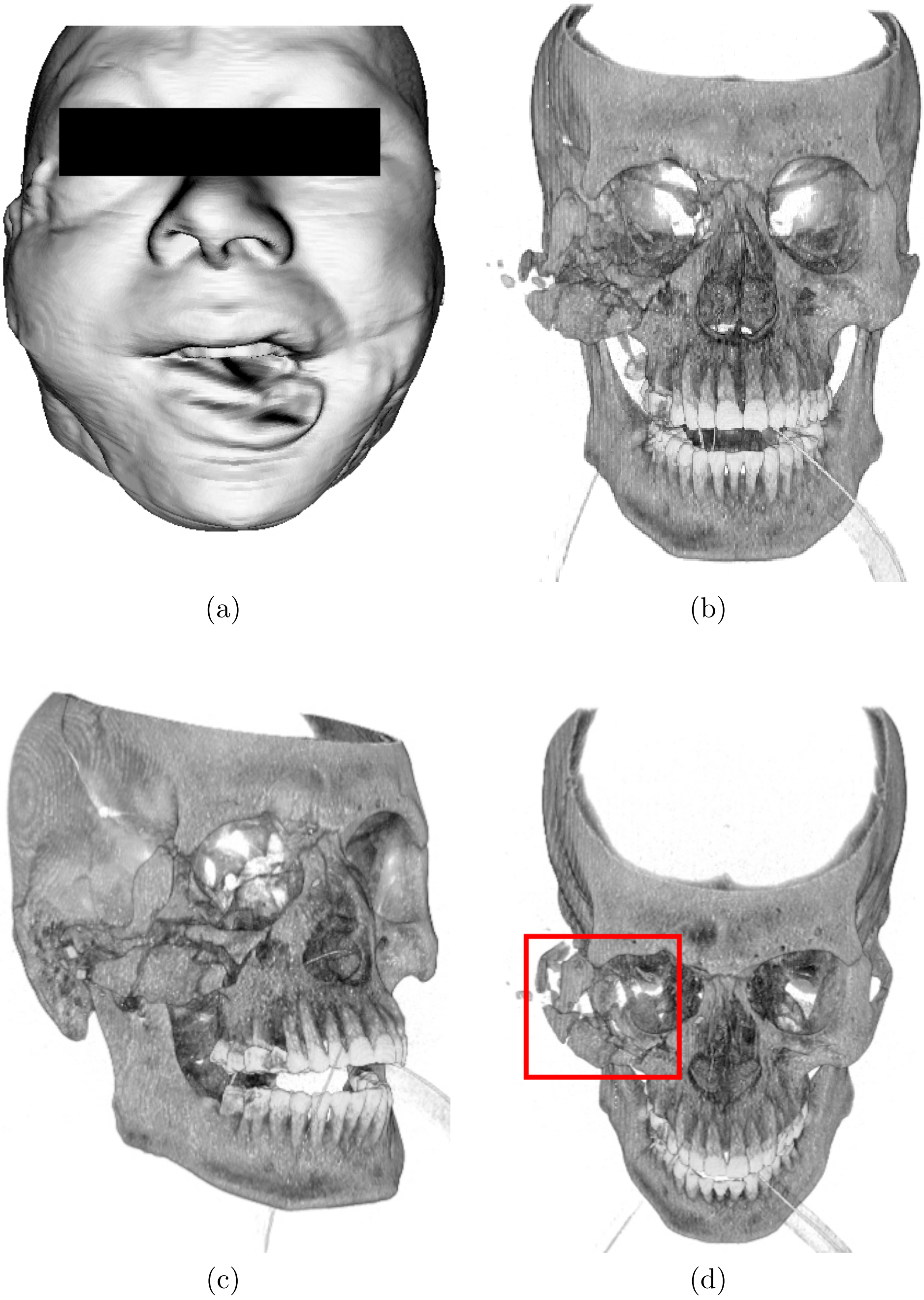

Figure 1.3: Skull deformity due to accident. (a) The deformed face. (b–d) The right part of patient's skull is severely fractured in an accident.

In CMF surgery planning, determination of the correct positions of the skull bones to restore the deformed skull is a very difficult procedure because information of the patient's normal skull is usually unavailable to the surgeon. For congenital deformity, the patient is born with a deformed skull. For deformity due to injury, the patient's normal skull before injury is typically unavailable unless he has undergone CT or MRI scan prior to the injury because of other head-related diseases. This difficulty often leads to unsatisfactory surgical results, with permanent functional and cosmetic deformities of the patients' face [Ltd06]. An example of an unsatisfactory CMF surgical result is shown in Figure 1.5. The surgery was performed on the same patient shown in Figure 1.4 before he was admitted to NUH. It was performed by an inexperienced CMF surgeon in a foreign hospital. After the surgery, the frontal part of the skull was still depressed, the patient's cheek bone was not properly restored, and the right side of the skull was still sunken. The patient was later admitted to NUH in which the correct CMF procedure was performed as discussed in the previous paragraph. To obtain good surgical results, pre-operative planning of CMF surgery, in particular the repositioning of bones, is essential.

Computer-aided systems have been developed to assist the surgeons in CMF surgery planning [LCL*02, AGG*03a, AGG*03b, ZGSZ03, AGG*04, MSB*06, KSS09, KGA*96, KGPG96, KGRG98, GEH*99, GWL99a, KRG*99, TGG99, CP00, BPM*00, XIS*00, XSC*00, GZDH01, CMPB02, TPS*02, GZDH03, LCL*03, MSCS03, CMC*04, GIR04, MSCP04, SBF*04, XGT05, ZLES05, DMCP*06, CSP*07, KSS09, SVBBC09, CTS*10, Mim, BCT*04, CBRY06, CBRY07]. These systems visualize medical images in 3D and simulate surgical operations such as cutting and repositioning of bones in the 3D models of the patients' skulls. Some systems attempt to simulate the reactions of the body in response to user inputs in real time to provide the user with realistic situations and perception of surgical procedures [LCL*02, AGG*03a, AGG*03b, ZGSZ03, AGG*04, MSB*06, KSS09]. Some other systems attempt to generate normal skull models of the patient for surgery planning guidance [GWL99a, LCL*03, ZLES05, DMCP*06, CSP*07, CTS*10, Mim]. Some systems can also estimate and evaluate post-operative facial appearance [KGA*96, KGPG96, KGRG98, KRG*99, TGG99, CP00, XIS*00, XSC*00, GZDH01, CMPB02, GZDH03, MSCS03, CMC*04, GIR04, MSCP04, SBF*04, SVBBC09].

However, these systems do not provide any means for assisting the surgeon to infer the optimal repositioning of the fractured bones of patients' skulls. The surgeons have to manually explore various options to determine the optimal repositioning of the bones. Several methods have been explored for the repositioning of bones. The method of Chowdhury, Bhandarkar et al. [BCT*04, CBRY06, CBRY07] determines the repositioning of bones for reconstruction of lower jaw by matching of fracture surfaces of adjacent bone fragments. Similarly, the method of Zhao et al. [WYLL11] determines the positions of the bone fragments of a victim by matching the fracture curves on the bone surfaces. These methods are, however, unreliable in the case of impact injuries resulting from traffic accidents, work accidents, home accidents, sports accidents, and violence. In these injuries, impact forces often cause the fracture surfaces to abrade each other, destroying the features for accurate matching [LP98].

1.2 Research Goal

The overall goal of this research is to develop a method for generating a CMF surgery plan for restoring a deformed skull back to a state with normal appearance. Limited by the data available, we focus on skull deformities due to trauma. The input of the method is the patient's 3D medical images. From these images, a 3D model of the injured skull called the **deformed model** is generated. The ideal normal state of the patient's skull before injury is called the **normal model**, which is generally unavailable in clinical practice.

A **reference model** is used to provide information about the normal appearance of a skull. This model can be either a 3D model of a single healthy skull or a statistical model of a population of healthy skulls. Theoretically, a statistical model contains more information about the possible variations of normal skulls than a single generic model. However, to build a good statistical model, many normal skull models must be collected. Therefore, as a start, a single normal skull model is used as the reference model. Statistical model will be considered later when enough normal skull models are available for constructing the statistical model. As 3D surface scanning is becoming more accessible, 3D face model of the patient before injury may also be used if it is available.

The output of the method consists of a **restored model** of the patient's skull and a **surgery plan** for obtaining the restored model by repositioning the bones in the deformed model. The restored model should be as close to the normal model as possible.

A CMF surgery planning system for skull injuries should assist the surgeon in deriving the surgery plan and the restored model. However, some existing systems produce only an estimate of the normal model, called the **reconstructed model** [GWL99a, LCL*03, ZLES05, DMCP*06, CSP*07, CTS*10, Mim], from the deformed model based on shape similarity. The detailed shapes of the bones in the reconstructed model are not necessarily the same as those in the deformed model. Therefore, it may not be possible to obtain the reconstructed model by repositioning the bones in the deformed model. Although the reconstructed model may be used as a reference guide during actual surgery, the surgeon needs to manually work out how to reposition the patient's bones to match the reference as given by the reconstructed model.

The proposed research focuses on the task of generating a surgery plan and the restored model. Its contributions include the following:

1. Develop a computer-aided procedure for assisting a surgeon in deriving a surgery plan for restoring a patient's deformed model back to the normal state. This procedure provides a practical way to transfer surgical constraints to computational constraints, so that, computer technologies can be applied to generate the CMF surgery plan

effectively and accurately.

2. Develop a method for generating the restored model from a patient's deformed model, which is the core algorithm in the proposed procedure. This method can be easily extended for restoration of other fractured rigid objects. It has potential application in other fields such as assembling of fractured potteries, chinaware and skulls in archeology.

1.3 Organization of Thesis Proposal

To understand the difficulties and detailed requirements of CMF surgery planning, it is necessary to first discuss in Chapter 2 the anatomy of the human skull, deformities of skulls, and CMF surgery for restoring deformed skulls. From the computational point of view, deriving the surgery plan is the most complex part of a surgery planning system. So, existing methods for reconstructing and restoring skull models are reviewed in Section 3.1. Existing systems and their methods for CMF surgery planning are then reviewed in Section 3.2. The proposed computer-aided CMF surgery planning procedure, the restoration problem, and its solution approach are described in Chapter 4, followed in Chapter 5 by preliminary work that contribute to the solution method. Chapter 6 concludes this thesis proposal.

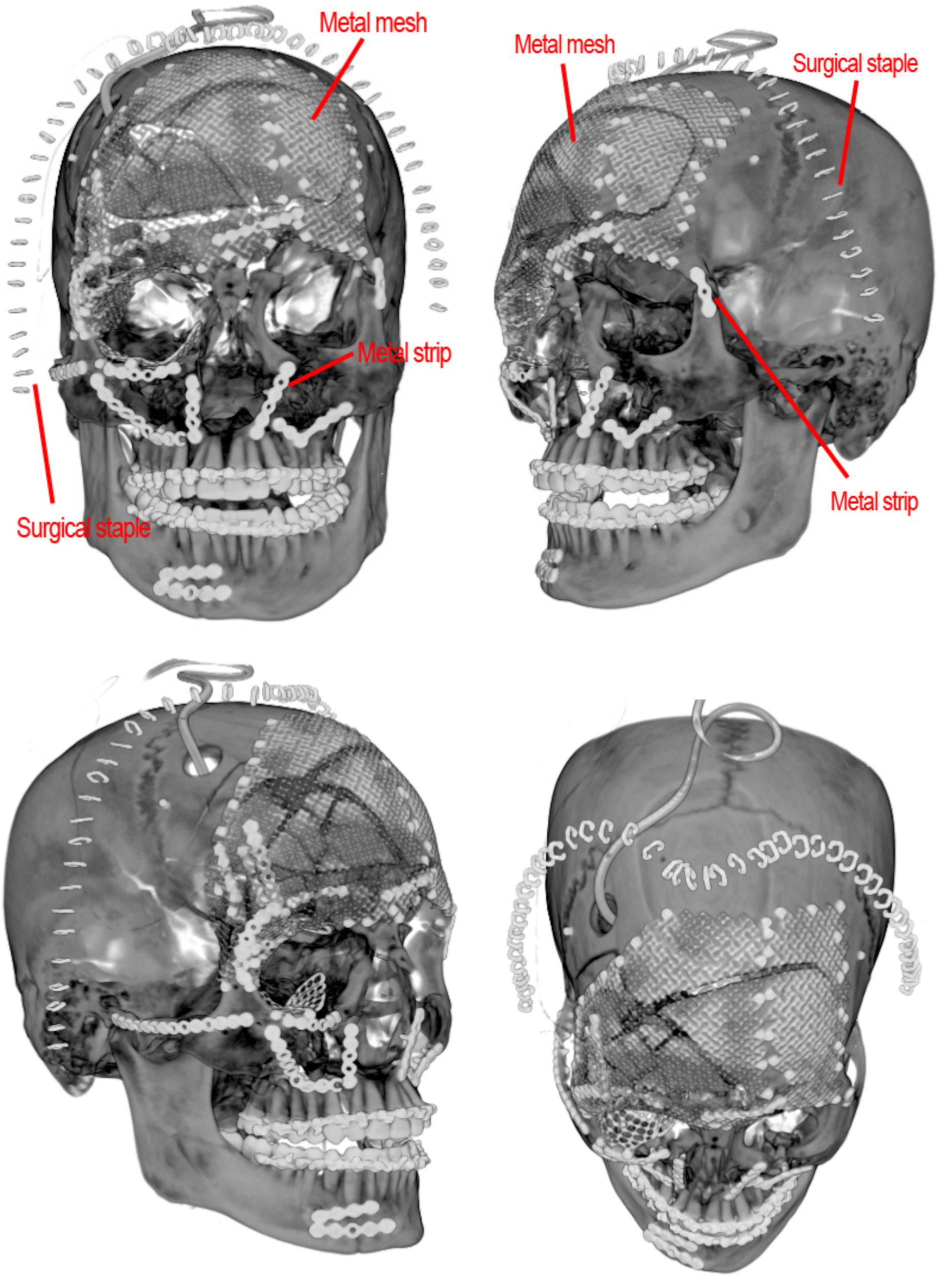

Figure 1.4: A satisfactory CMF surgery result. It correctly restored the skull to normal appearance. Surgical staples are used to close the skin. Metal strips and metal meshes are used to fix the bones.

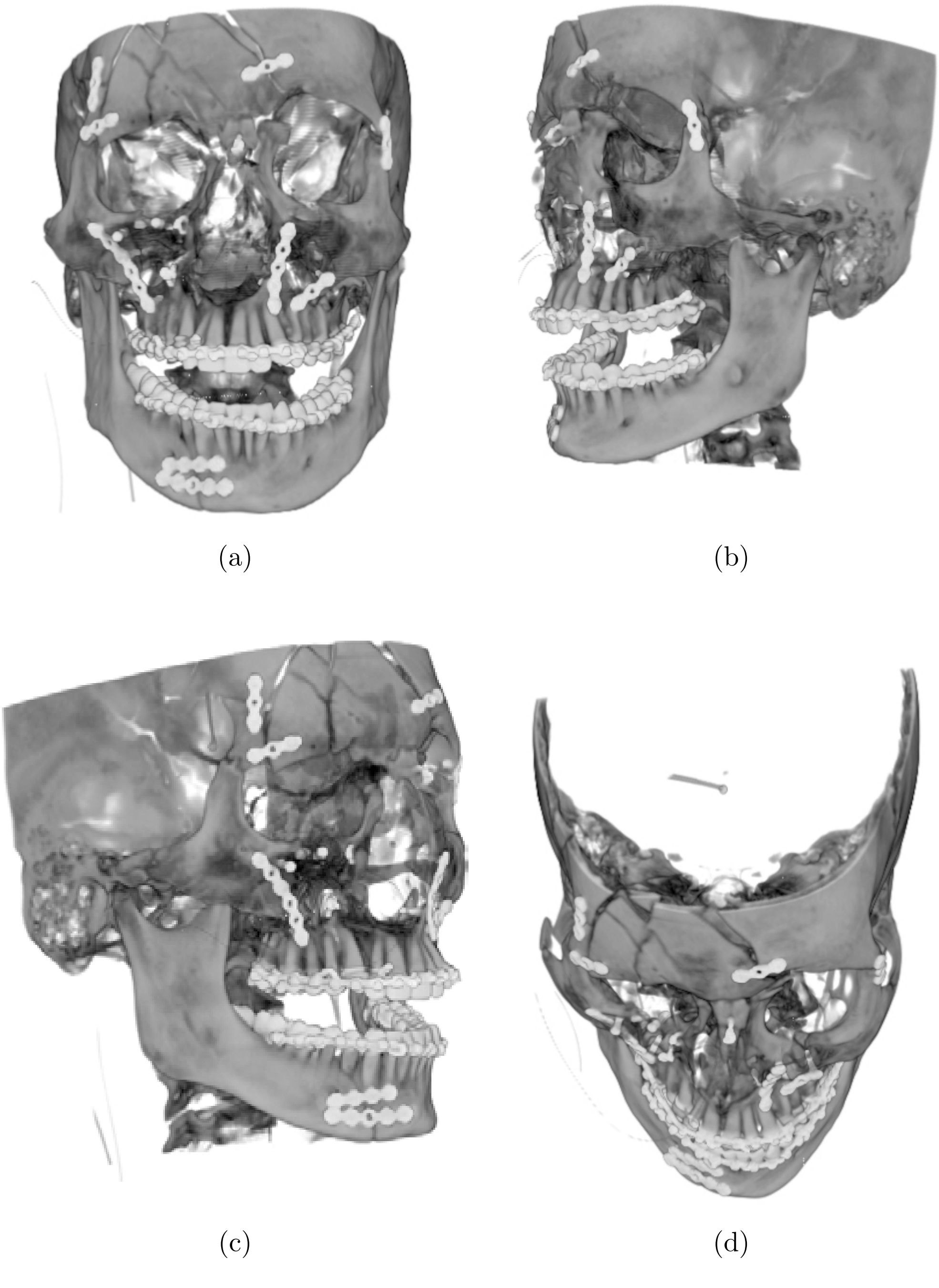

(a) (b) (c) (d)

Figure 1.5: An unsatisfactory CMF Surgery result. Bones are not correctly repositioned, causing the right side of the skull to be set back.

Chapter 2

Background

This section provides background knowledge that serves as the basis of further discussion. First, the anatomy of the skull is presented in Section 2.1. Next, two important virtual planes that define the skull orientations and landmarks are discussed in Section 2.2. Next, skull deformities are briefly discussed in Section 2.3. Finally, CMF surgery for correcting skull deformity is described in Section 2.4.

2.1 Skull

The skull is a 3D structure consisting of 28 bones that are fused together [SH]. While its general shape is similar for all normal humans, it can vary greatly in size and shape details among different individuals, resulting in the variation of facial appearance of people in different age, gender and ethnic groups.

Excluding three pairs of small auditory ossicles (the small bones in the ear canals transmitting sound), the other 22 skull bones can be divided into two groups, the cranial bones and the facial bones [Wik09]. 8 cranial bones fuse together to form the cranial cavity that contains and protects the brain. 14 facial bones form the mechanical framework of the face, and provide the attaching sites for the facial muscles. Based on their positions, the 14 facial bones together with the frontal cranial bone are divided into three groups, namely the upper third (frontal bone), middle third (from the frontal bone down to the upper jaw) and lower third (the lower jaw).

Most of the skull bones are fixed. The only exception is the jaw structure that provide chewing function. The upper jaw, maxilla, is fused with the zygomatic (cheek) bones and other bones. The lower jaw, mandible, connects to the two temporal bones. The temporomandibular joints between them are the only joints that allow movement of the

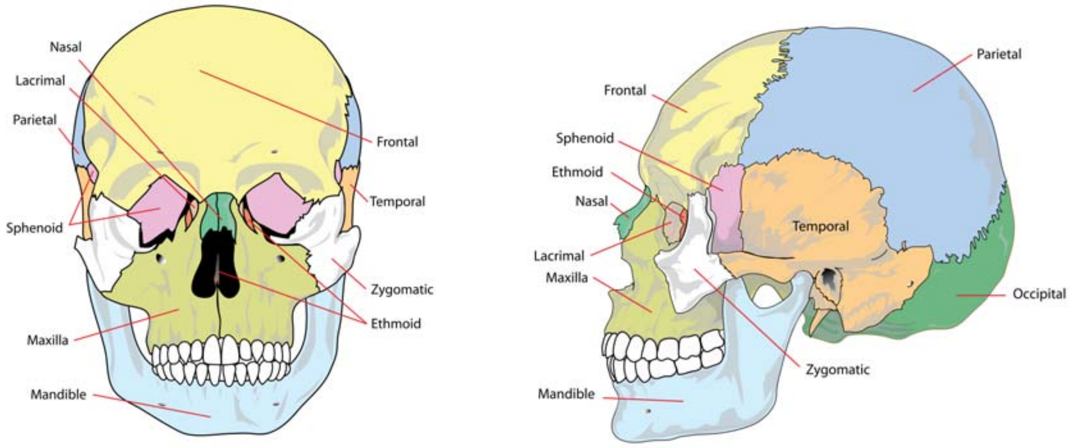

(a) (b)

Figure 2.1: Skull bones [Wik09]. (a) Frontal view. (b) Side view. The skull consists of 28 bones fused together.

lower jaw relative to the upper jaw.

2.2 Important Planes of the Skull

The Frankfurt Plane (FP) and the Mid-Sagittal Plane (MSP) of a skull (Figure 2.2) are very important in surgery, forensics, and anthropology. They are used to define the three anatomical orientations of the skull. The lateral (left-right) direction is normal to the MSP, the superior-inferior (up-down) direction is normal to FP, and the anterior-posterior (front-back) direction is parallel to the intersection line of FP and MSP. These anatomical orientations, in turn, are used to define craniometric landmarks that are used for pre-operative surgery planning, intra-operative surgery guidance, forensic reconstruction, and anthropological and archaeological studies [CHV99, DMCP*06, GWL99b, SH, Tay01, Woo31].

In anatomy, the FP is defined as a plane that passes through the orbitales and the porions [AAG09] (Figure 2.2). The left and right orbitales (Ol, Or) are the lowest points of the lower margin of the left and right orbits (eye sockets). The left and right porions (Pl, Pr) are the most lateral points of the roofs of the left and right ear canals.

The MSP is defined as a vertical plane that passes the midline of the skull [AAG09]. A number of features lie on the skull's midline. Based on the landmarks used in anatomy [SH] and forensics [Tay01], 6 landmarks are selected to define the midline (Figure 2.2) in our preliminary work [CLL11]:

1. The nasal bone suture (NR) is a ridge structure formed by the joint of the left and right nasal bones.

2. The mid-philtrum ridge (MPR) is a ridge structure along the anterior (front) nasal spine towards the upper lip margin.

3. The posterior nasal spine (PNS) is the peak at the posterior end of the median palatine suture, which is the joint of the left and right palatine bones.

4. The vomer ridge (VR) is a ridge structure at the vomer, which forms a part of the nasal septum (the bone that divides the nose into the left and right airways).

5. The foramen magnum center (FMC) is the center of foramen magnum, a circular opening at the bottom of the skull where the spinal cord passes through.

6. The external occipital crest (EOC) is a ridge structure along the midline at the bottom of the skull.

The ridges lie on or close to MSP. For the purpose of defining the MSP, we can use an estimate of the ridges centroid as the ridge landmark point.

The skull is divided into the left and right halves by the MSP. The general structure and shape of the two sides are roughly similar. Therefore, the MSP is sometimes considered as the symmetric plane of the skull [DMCP*06]. However, extensive studies show that there is significant asymmetry in the human skull [RRS03, Woo31].

2.3 Skull Deformities

Skull deformities refer to shape distortions of the skull. They may be traumatically acquired in traffic accidents, work accidents, home accidents, sports accidents, or violence, or congenitally malformed at birth. As the proposed research focuses on skull deformities due to injuries, congenitally malformed deformities are omitted in this discussion.

Traumatic deformities to different parts of the skull have different type of features [LP98] (Figure 2.3). Deformities to the upper part of the skull are usually linear cracks or bony depressions over the frontal sinuses, the empty gap in the frontal region of the frontal bone (Figure 2.3).

Serve deformities of the middle part of the facial bone can result in the detachment of the bone, and the bone is thrust backward down the inclined slope of the base of the skull. This will cause flattened face. For the example, in Figure 2.3, the right zygomatic arch, a bony structure formed by the forward extending part of the temporal bone and the side of

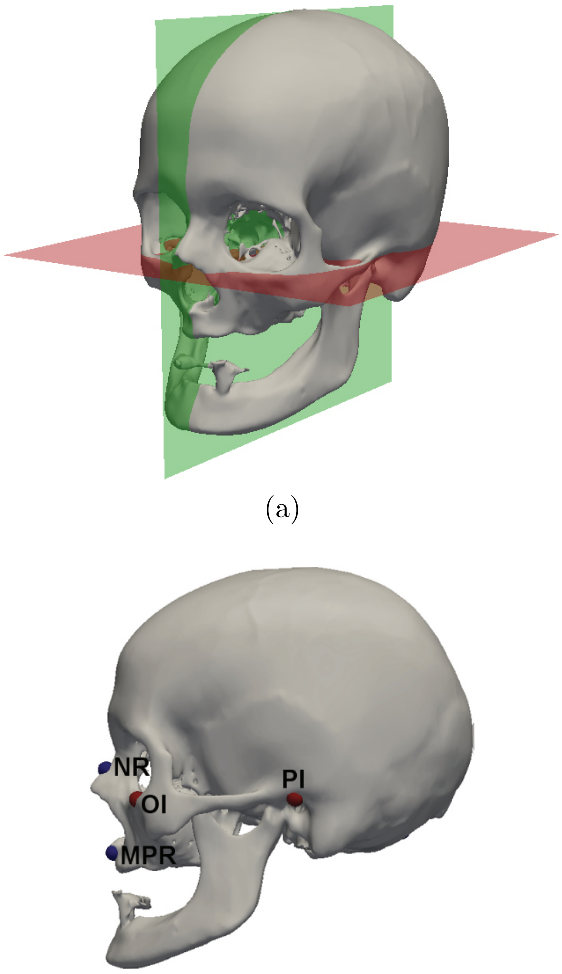

(a) (b) (c) (d)

Figure 2.2: Frankfurt plane, mid-sagittal plane, and craniometric landmarks. (a) The Frankfurt plane (FP) is the horizontal (red) plane, and the mid-sagittal plane (MSP) is the vertical (green) plane. (b–d) The red landmarks are the landmarks that define the FP. The blue landmarks are the landmarks that define the MSP.

the zygmatic bone, is broken into several small fragments and displaced backward. More dangerously, the fractured and displaced bones near the airway may close off the airway, which threatens the life of the patient. Moreover, these fractures may cause permanent damage such as compression and folding of the thin bones in the nose and orbit, which cannot be reconstructed by CMF surgery.

Fractures to the lower part of the skull occur in many positions of the mandible. They are mainly cracks, displacements and smashes. The mandible of the patient shown in Figure 2.3 is broken into fragments, which are displaced from their original positions.

2.4 CMF Surgery

Craniomaxillofacial (CMF) surgery aims to restore a deformed skull back to its normal state. More specifically, its resulting skull should be normal in anatomy. In addition, the MSP of the skull should be restored and the whole skull should be symmetric with respect to the restored MSP.

The CMF surgery involves very complex operations on the skull bones [LP98, Ltd06]. This section describes the CMF surgery operations that were applied to the patient in Figure 2.3, as explained by the surgeon.

Figure 2.4 illustrates the CMF operations on the patient. In the top part of the skull, the fractured frontal bones were located and pulled forward to a new position and a new orientation to restore the normal shape (Figure 2.4, first and second row).

Operations to the middle part of the skull is more complex. The zygomatic (cheek) bone was moved forward and downward, rotated a bit and fixed to the new position using plates, restoring a normal zygomatic arch shape connecting the zygmatic bone and the temporal bone (Figure 2.4, third row). To provide support to the eye balls, metal meshes are fixed to the lower orbital roof (Figure 2.4, fourth row). In addition, in order to hold the upper jaw, the maxillae, in proper position while healing, metal plates were used to fix the maxilla bone to the zygomatic bones (Figure 2.4, fifth row).

In the lower part of the skull, the surgeon estimated the original positions of the two fractured bone fragments of the lower jaw. Then, he moved them and fixed them at the estimated original positions.

Figure 2.5 shows the result of the CMF surgery. As can be seen, after the complex CMF operations, the overall shapes of the skull and the face were restored to a more normal and symmetric state.

It is worth noting that some bone fragment are not operated on though they are

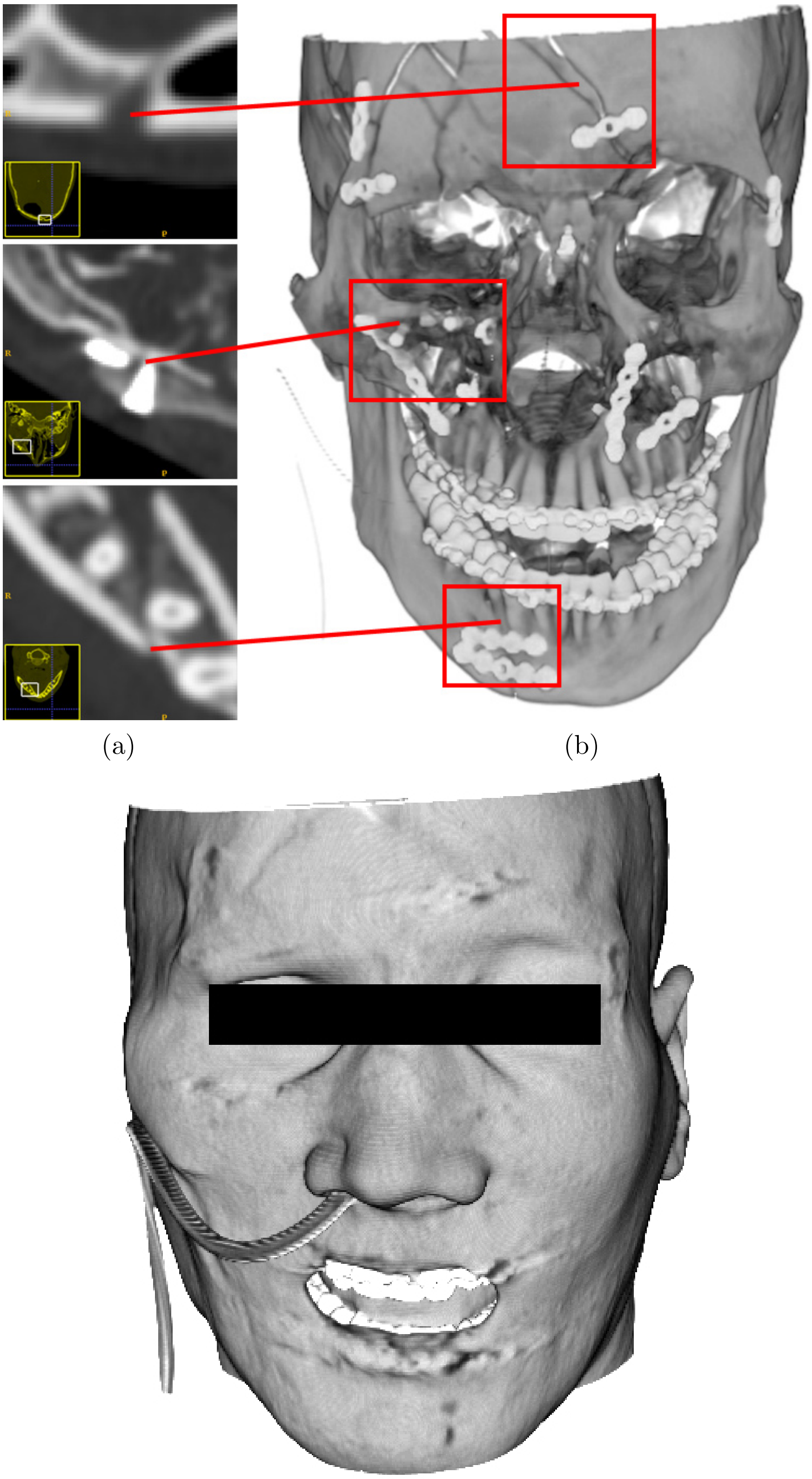

(a) (b)

(c)

Figure 2.3: Skull deformities. (a) CT images showing various deformities. (b) 3D volume rendering of the skull. (c) 3D volume rendering of the skin.

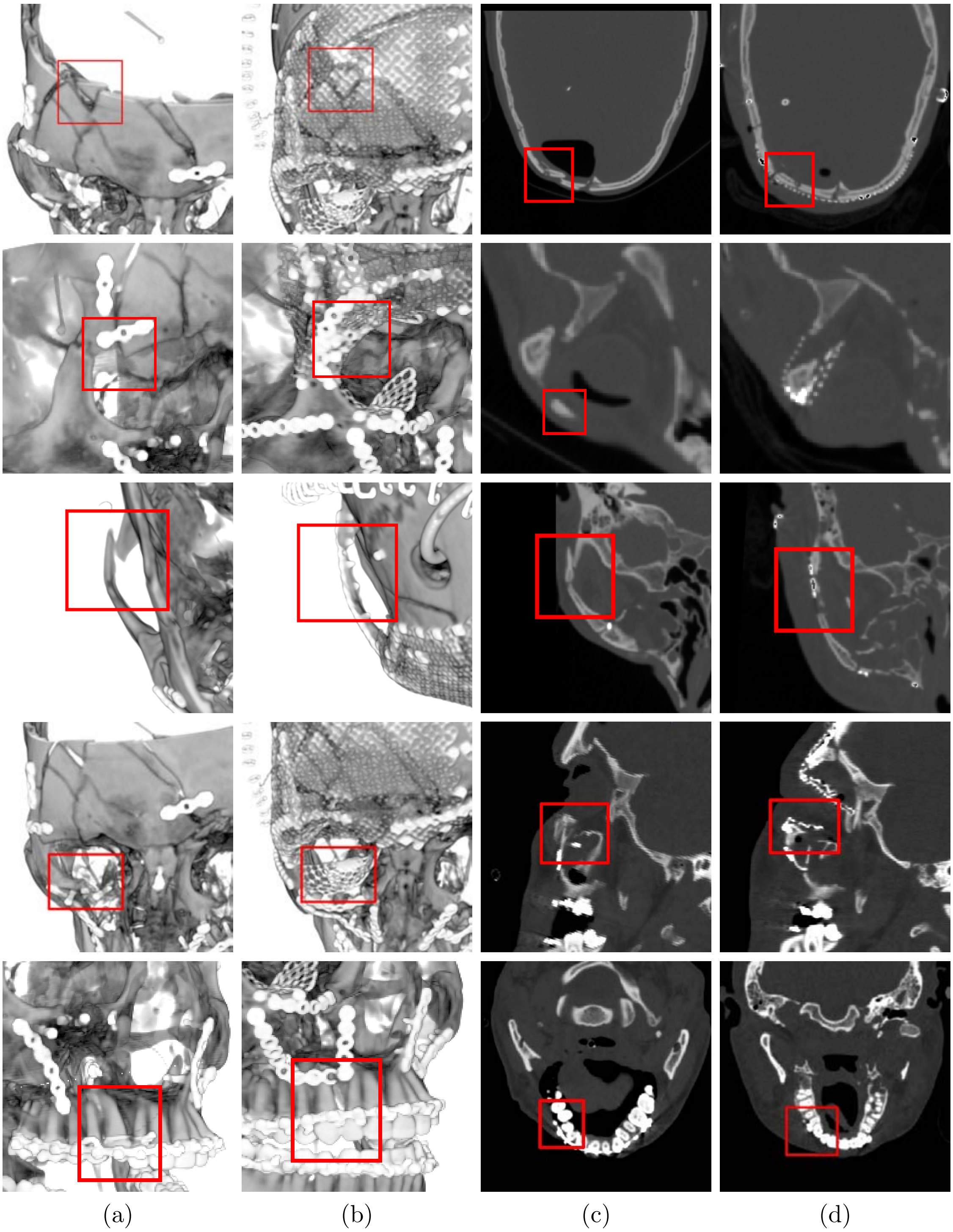

Figure 2.4: CMF surgery one deformed skull. (a) Volume rendering of pre-operative skull. (b) Volume rendering of post-operative skull. (c) CT slice of the pre-operative skull. (d) CT slice of the post-operative skull. (Row 1) Frontal bone region. (Row 2) Upper right orbital region. (Row 3) Right zygmatic arch region. (Row 4) Lower right orbital region. (Row 5) Maxilla bone.

affected by the fracture. This is mainly because of some clinical considerations. For example, some bones are broken into very small fragments. The position of these small bone fragments have little affect on the overall structure of the resulting skull. In addition, though fractured, some other fragments are not displaced very much (Figure 2.6). They are still close to the correct position, and they also do not affect the overall structure too much. Therefore, it is not worthy to open the fragment and operate on them.

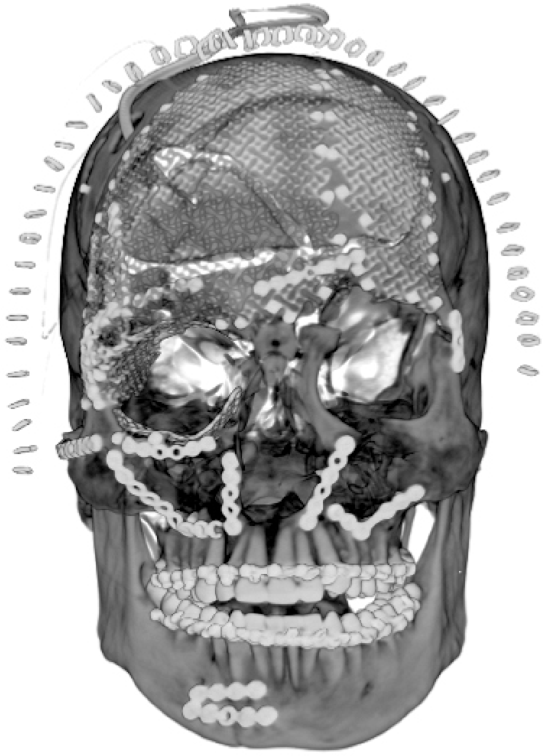

(a)

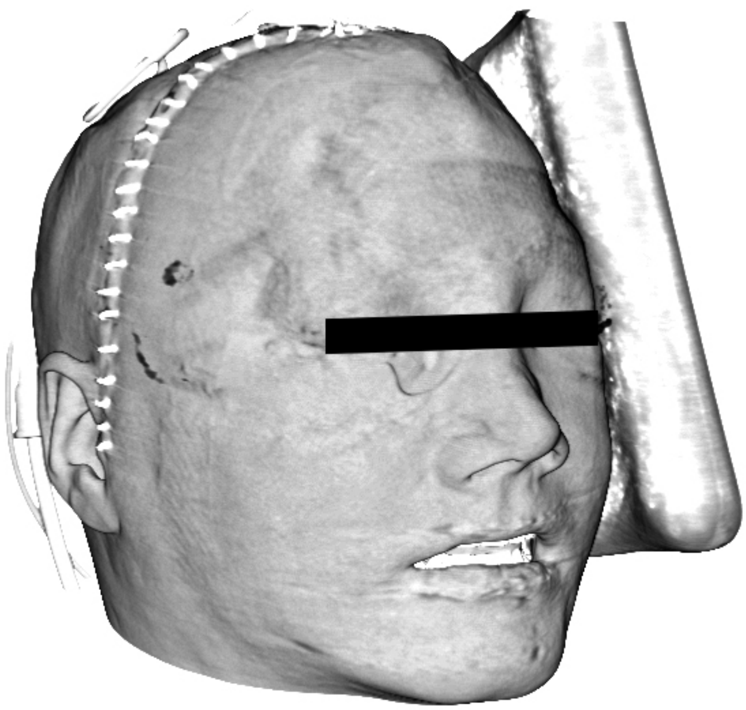

(b)

Figure 2.5: Result of CMF surgery. (a) The post-operative skull. (b) The post-operative face.

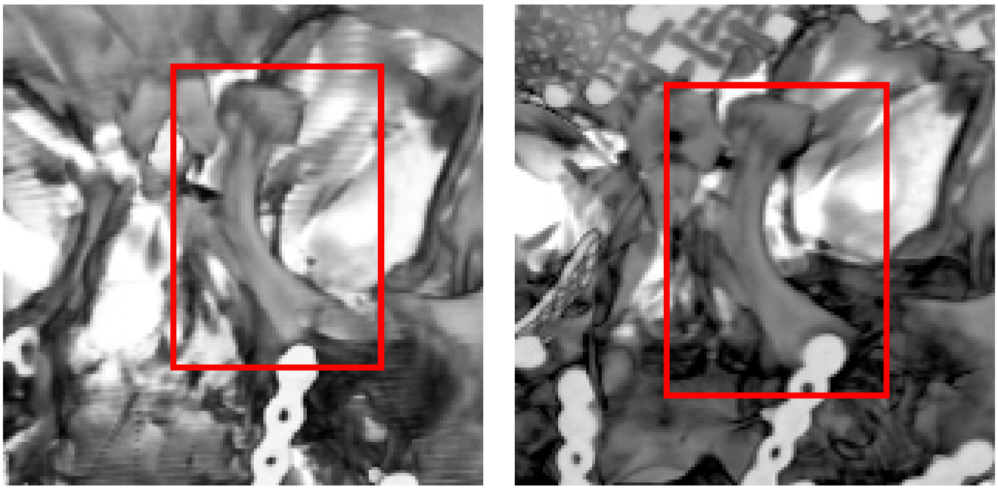

(a) (b)

Figure 2.6: Bone fragment not moved in surgery. (a) Pre-operative. (b) Post-operative.

Chapter 3

Related Work

As discussed in Section 1.2, there are two related problems in CMF surgery planning, namely restoration and reconstruction. Section 3.1 reviews existing work for restoration and reconstruction. Some of these methods have been applied in existing systems for CMF surgery and orthodontics (dental) surgery. These systems are reviewed in Section 3.2.

3.1 Restoration and Reconstruction

Model restoration seeks to restore the deformed model back to its normal state by repositioning the bones in the deformed model. Model reconstruction, on the other hand, derives an estimate of the normal model from the deformed model by shape similarity. There are currently two restoration methods, namely manual manipulation and fracture surface matching, and three reconstruction methods, namely symmetry-based reconstruction, geometric reconstruction, and statistical reconstruction. The following sections discuss these methods in increasing order of complexity.

3.1.1 Manual Manipulation

Manual manipulation methods display the 3D model of a patient's skull in the computer monitor and allow the surgeon to virtually cut and reposition the bones in the 3D model [KGA*96, KGPG96, KGRG98, GEH*99, GWL99a, KRG*99, TGG99, CP00, BPM*00, XIS*00, XSC*00, GZDH01, CMPB02, TPS*02, GZDH03, LCL*03, MSCS03, CMC*04, GIR04, MSCP04, SBF*04, XGT05, ZLES05, DMCP*06, CSP*07, KSS09, SVBBC09, CTS*10, Mim]. They provide user interfaces for the surgeon to operate on 3D models of bones and manually determine the surgery plan. For example, Figure 3.1 shows a planning system based on manual manipulation [XGT05]. The system allows the user to virtually cut and

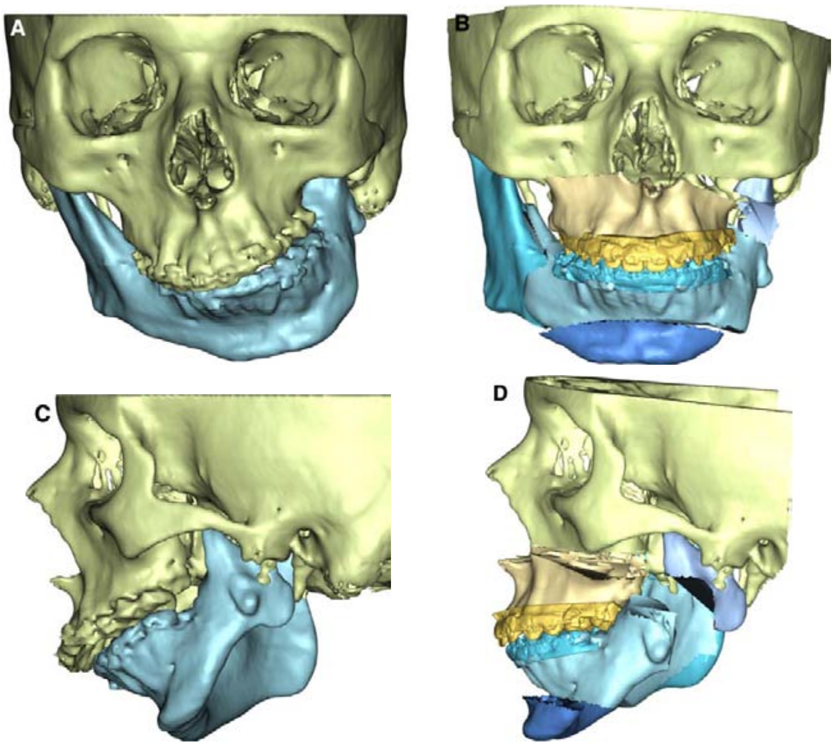

Figure 3.1: Manual restoration [XGT05]. (a,c) Deformed model. (b,d) Restored model after cutting and repositioning of bones.

displace bones, and renders the resulting skull shape for visual examination. Some systems provide additional features to assist the surgeon in manual manipulation. These features include anatomical measurements such as relative position and angle between anatomical landmarks [BPM*00, CMPB02, TPS*02, XGT05, CSP*07], collision detection [GEH*99, TPS*02], post-operative facial tissue prediction [KGA*96, KGPG96, KGRG98, KRG*99, TGG99, CP00, XIS*00, XSC*00, GZDH01, CMPB02, GZDH03, MSCS03, CMC*04, GIR04, MSCP04, SBF*04, SVBBC09] and generation of reconstructed model [GWL99a, LCL*03, ZLES05, DMCP*06, CSP*07, CTS*10, Mim]. They facilitate the planning procedure and improve manual manipulation accuracy.

Manual manipulation method is relatively easy to implement. It gives the surgeon maximum control over how the bones in the deformed model should be repositioned. Some systems provide additional features to assist the surgeon. Nevertheless, it is quite tedious for the surgeon to manually explore various possibilities. It also requires an experience surgeon to visually assess whether the restored model is satisfactory.

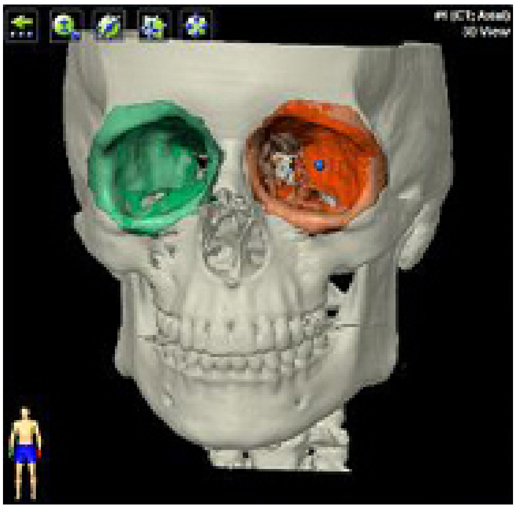

Figure 3.2: Symmetry-based reconstruction [GWL99a]. The skull model is colored white. The green region on the right side is reflected and overlaid onto the left side as the orange region.

3.1.2 Symmetry-Based Reconstruction

Symmetry-based methods produce a reconstructed model based on left-right symmetry of the human skull [GWL99a, LCL*03, DMCP*06, CSP*07, CTS*10, WYLL11, Mim]. These methods require the user to indicate the healthy regions of the deformed model (Figure 3.2, green part). Then they reflect the healthy parts with respect to the Mid-Sagittal Plane (MSP). This reflection (Figure 3.2, orange part) serves as an estimation of the normal state of the deformed parts, and is used to generate the reconstructed model. Symmetry-based method is applied in Brainlab [GWL99a], a leading CMF surgery planning system used in NUH. Brainlab does not reconstruct the whole skull model. Instead, it just reflects the healthy parts identified by the user, which are then regarded as the reference for actual surgery. Thus, Brainlab can be regarded as producing a partially reconstructed model.

In symmetry-based methods, correct identification of MSP is essential to the accuracy of reconstruction. Semi-automatic methods have been designed to identify MSP [CSP*07, CTS*10, DMCP*06]. In the work of [DMCP*06], two methods were proposed. The first method requires the user to indicate the points on the MSP and/or laterally symmetric points on both sides of the skull (Figure 3.3(a)). Then, it fits a plane over the points as the MSP. The second method requires the user to indicate laterally symmetric parts on both sides of the skull using a virtual brush (Figure 3.3(b)). Then, it determines the mirror reflection plane between the left and right parts, which is regarded as the MSP.

Symmetry-based reconstruction uses the natural approximate left-right symmetry of the human skull. It requires the presence of healthy bones to reconstruct the fractured

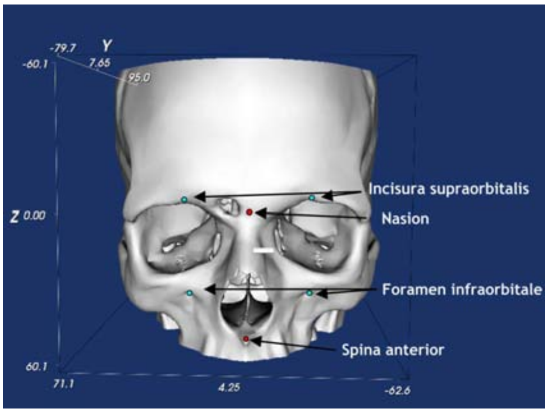

(a)

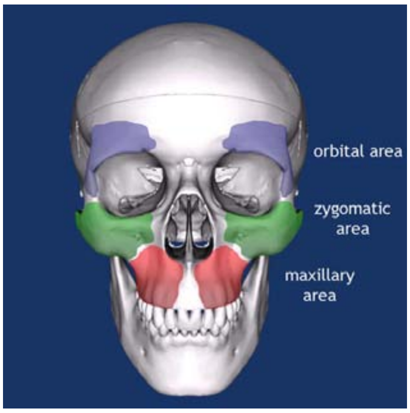

(b)

Figure 3.3: Semi-automatic methods for identifying the MSP [DMCP*06]. (a) Red landmarks are the MSP landmarks given by user, and the blue landmarks given by user are symmetric to MSP. (b) Regions with the same color are the symmetric regions indicated by user.

parts on the opposite side of the skull. When both sides of the skull are fractured, which is common in impact injuries, this method cannot be applied.

3.1.3 Geometric Reconstruction

Geometric reconstruction methods use generic shape models to estimate the normal shape of the deformed part [GMBW04, BSMG09, WYLL11]. They deform the generic model to match the healthy parts of the deformed model. Then they apply a generic shape function to interpolate the fractured or missing parts to generate the reconstructed model. For example, [GMBW04] applies thin-plate spline to deform a reference model and register it to the model with missing parts (Figure 3.4(a)). After registration, the missing parts are filled in by the registered reference model (Figure 3.4(d)) .

Geometric reconstruction is relatively simple to apply. However, detailed shapes of human skulls vary significantly across different gender, age and ethnic groups. Selection of a reference model in the same gender, age and ethnic group is essential for reconstruction accuracy [GMBW04]. Lack of similar reference model will affect the reconstruction result. In addition, geometric reconstruction uses the correlation between the healthy parts and the deformed parts, which is weak for severely deformed model. In some severely deformed models, the whole frontal face is deformed (Figure 1.5), leaving only the back of the skull healthy. The correlation between the back portion and the frontal portion is weak. Therefore, in such case, the geometric reconstruction generates a model whose frontal face is close to the reference model, instead of the patient's normal model.

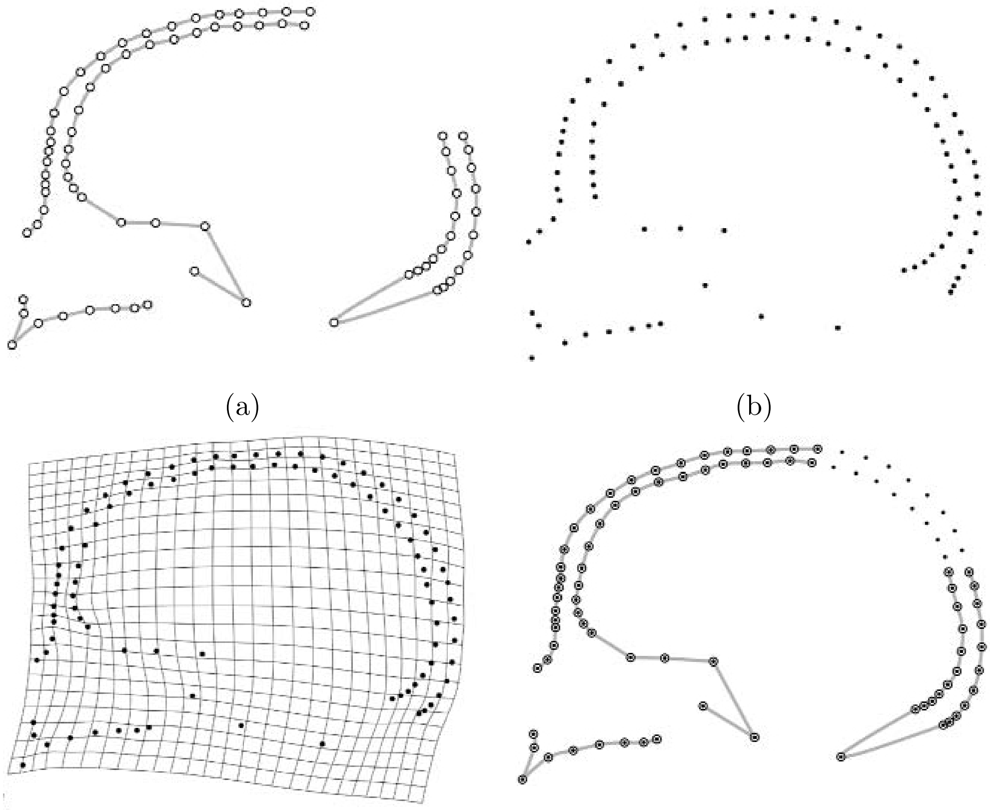

(a) (b) (c) (d)

Figure 3.4: Geometric-based reconstruction [GMBW04]. (a) A model with missing parts. (b) A reference model. (c) Thin-plate spline deformation of (b) registered to (a). (d) Reconstructed model with the missing parts filled in by the registered reference model.

3.1.4 Statistical Reconstruction

Statistical reconstruction methods match a statistical reference model to the healthy parts of a deformed model and use the matched statistical model to infer the fractured parts of the deformed model [Phi05, ZLES05, BSMG09, LAV09]. For example, given a set of training samples of healthy mandibles, the method in [ZLES05] applies Principal Component Analysis (PCA) to compute the mean shape and the principal variation modes of the training samples. Next, it computes the principal variation modes that best match the statistical model to the healthy parts of a patient's deformed model. Finally, it uses the computed principal variation modes to generate a reconstructed model from the statistical model.

Statistical reconstruction overcomes the limitation of geometric reconstruction by capturing normal variations of human skulls in the statistical reference model. It can potentially produce a reconstructed model that is close to the normal model of a patient, provided that a good match is obtained between the patient's deformed model and the

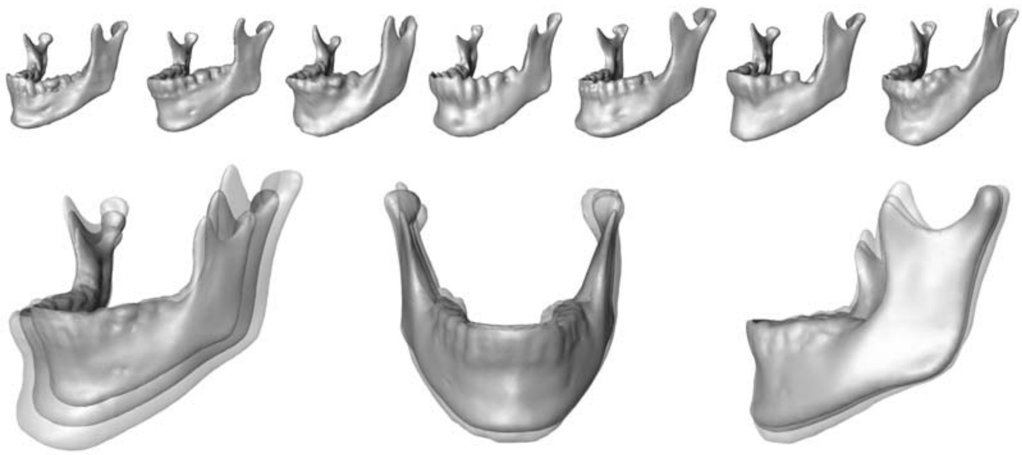

Figure 3.5: Statistical mandible shape model [ZLES05]. (Top) Training samples. (Bottom) Three main variation modes of the statistical model.

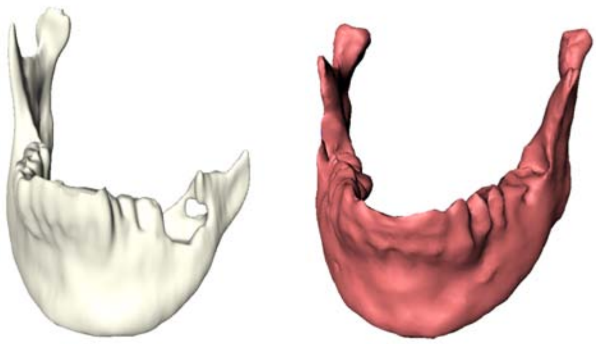

(a) (b)

Figure 3.6: Statistical reconstruction of mandible [ZLES05]. (a) Model of patient's deformed mandible. (b) Reconstructed model.

statistical reference model. However, one potential limitation is that the construction of the statistical reference model requires a large amount of training samples of healthy skull models, preferably categorized into various gender, age, and ethnic groups. Their reconstruction accuracy depends on how well the statistical model captures the normal shape variation of the patients' normal model. In the case that such normal shape variation is not adequately captured, then only the mean shape of the statistical reference can be used. Then, statistical reconstruction becomes geometric reconstruction. Insufficient training samples will affect the reconstruction result. In addition, statistical reconstruction methods are also based on the correlation between between health parts and deformed parts. For severely deformed models with only a small healthy portion, statistical methods can only generate a model which is close to the training samples mean shape in the deformed regions.

(a) (b)

Figure 3.7: Fracture surface matching method [CBRY06]. (a) Cross section of a bone that is fractured into two fragments. (b) The fragment on the left is repositioned at the correct position and orientation relative to the one on the right.

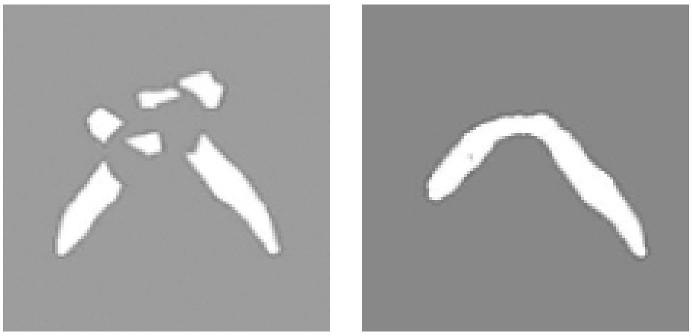

(a) (b)

Figure 3.8: Fracture surface matching method one multiple fracture case [BCT*04]. (a) Cross section of a bone that is fractured into multiple fragments. (b) Restored model computed by repositioning the fragments at their correct relative positions and orientations.

3.1.5 Fracture Surface Matching

Fracture surface matching methods reposition fractured bones by determining their correct relative positions and orientations based on shape complementarity of adjacent fracture surfaces. Shape complementary is measured by the mean distance between the corresponding points of two adjacent surfaces. These methods first compute the rigid transformations that brings the adjacent fracture surfaces into registration that maximizes shape complementarity. The rigid transformations determine the relative positions and orientations of two adjacent bone fragments. This method is applied in the work of Chowdhury, Bhandarkar et al. [BCT*04, CBRY06, CBRY07] to restore mandible fractures. It uses an algorithm inspired by RANSAC to determine a subset of corresponding vertices of the two fracture surfaces that best align them. After this initial alignment, it further refines the fracture surface alignment by ICP algorithm [BM92] over all the vertices. It then applies the transformation between the two fracture surfaces to restore the mandible shape (Figure 3.7).

In cases where multiple fractures occur, more that one pair of fracture surfaces exist. Determining the correspondence of adjacent fracture surfaces is also important. The work in [CBRY06] solves this problem using graph method. It formulates the problem as a maximum weighted graph matching problem. Each fracture surface corresponds to a node in the graph. The edge between two nodes is assigned a weight measuring the shape complementarity of the two fracture surfaces of the two nodes. These nodes and weighted edges form the graph. A matching of a graph is a set of edges such that no two edges in it are incident on the same vertex. Thus a matching gives the corresponding fracture surface pairs. Edmonds's algorithm [Edm65] is applied to solve the problem in polynomial time (Figure 3.8).

In [WYLL11], Zhao et al. proposed a similar method for automatic assembly of fragmented skulls in archaeological and anthropological applications. This method represents the skull by its outer surface with zero thickness instead of a solid model. So a fracture is represented by a curve instead of surfaces. This method first uses ICP algorithm to roughly register the skull fragments to a reference skull. Then, it refines the result by registering neighboring fragments based on the matching of their fracture curves.

In contrast to methods discussed in the previous sections that produce only a reconstructed model, fracture surface matching methods produce a restored model by computing the correct positions and orientations of the fractured bone fragments. However, they require the features of fracture surfaces to be well preserved so that accurate shape complementarity can be computed. In the case of impact injuries, the fracture surfaces may abrade each other obliterating their surface features [LP98]. In this case, fracture surface matching becomes inaccurate and unsuitable for surgery planning. So far, it has been applied only to the planning of mandible restoration [BCT*04, CBRY06, CBRY07]. In contrast, this proposal presents an automatic, reliable and accurate method for generating the restored model.

3.2 Computer-Aided Surgery Planning Systems

CMF surgery operates on the skull whereas orthodontics surgery operates on the jaws and teeth. As both types of surgery are related, this section reviews existing computer-aided surgery planning systems for both of them. These systems are categorized into reactive systems (Section 3.2.1) and predictive systems (Section 3.2.2).

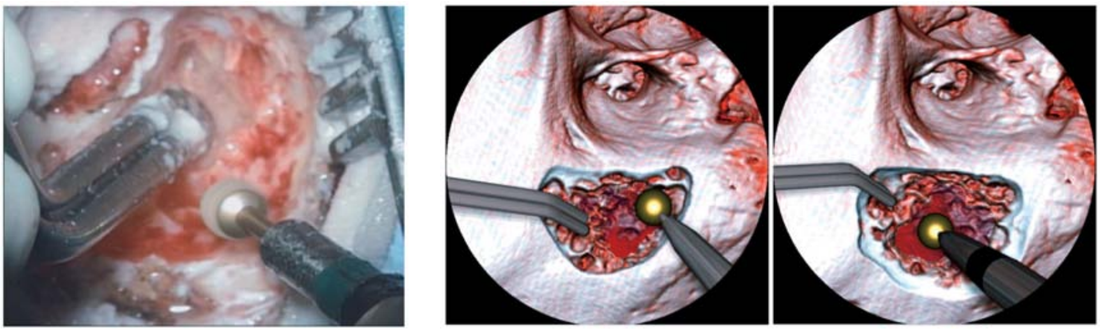

(a) (b)

Figure 3.9: Reactive system that simulates bone removal operation [KSS09]. (a) Typical view in real surgical procedure. (b) Screen shots of the reactive system.

3.2.1 Reactive Systems

Reactive systems are real-time systems that attempt to simulate the reactions of the body in response to user inputs [LCL*02, AGG*03a, AGG*03b, ZGSZ03, AGG*04, MSB*06, KSS09]. The user inputs emulate surgical operations such as cutting, drilling, moving, and fixing of bones. The systems simulate body reactions such as change of bone shape, displacements of bones, bleeding, etc. The objective of reactive system is to provide the user with realistic situations and perception of surgical procedures, through user interactions and simulated reactions of the body.

Reactive systems have been developed for skull surgeries. For example, Kerwin et al. [KSS09] developed a reactive system for simulating the removal of the bone behind the ear. Figure 3.9(a) shows a real image taken in an operation theater. It is the typical view that a surgeon would have during the procedure. The reactive system shown in Figure 3.9(b) aims to provide a realistic feel for the user. To achieve this, it provides the user with virtual tools such as bone drilling tool, irrigation tool and suction tool, that emulate real surgical tools, and provides the user with haptic feedback and sound cues of tool usage. The system also simulates the change of bone shape and bleeding in response to drilling in real time to enhance the experience. The system of Agus et al. [AGG*03a, AGG*03b, AGG*04] provides the same user experience. For general CMF surgery, the system of Morris et al. [MSB*06] provides visual and haptic feedback for surgical operations such as drilling, cutting, moving of bone fragments, and attaching of rigid metal plates.

Reactive systems are useful for medical training and pre-operative planning of basic surgical operations. They are not suitable for pre-operative planning of complex surgical procedures such as the whole CMF surgery. To use a reactive system to plan a complex procedure and predict the surgical results, the user would need to go through all the delicate operations in the procedure, which is very tedious and time-consuming.

3.2.2 Predictive Systems

Predictive systems attempt to accurately predict surgical results of complex surgical procedures based on predefined or user-specified surgical requirements. Depending on the design of the predictive systems, the user inputs to the systems can consist of surgical requirements like desired facial shape, implant shape, bone cutting position, etc. The surgical results provided by predictive systems can be the resultant skull model or the deformed facial surface. The objective of predictive systems is to allow the user to easily explore various surgical options to determine the best surgery plan.

Compared to reactive systems, predictive systems are designed to plan entire surgical procedures such as the whole CMF surgery instead of simulating basic surgical operations. In predictive systems, real-time response is not a necessary requirement. Instead, accurate surgery planning and effective assessment of the surgical results are very important.

Predictive simulation systems have been developed for pre-operative planning of orthodontics surgery and surgical implants [VvCM*96, DGL*01, TVE*07, CSP*07]. The system of Verstreken et al. [VvCM*96] allows a surgeon to manually manipulate dental implant model in either 3D or 2D. The system of Dutreuil et al. [DGL*01] allows a surgeon to validate dental implant shape by rendering the 3D data in the view defined by the surgeon. The system of Bettega et al. [BPM*00] allows a surgeon to manually reposition the bones in the upper jaw and perform dental analysis on the model for evaluation. The system of Chapuis et al. [CSP*07] provides a symmetry-based method for generating a reconstructed model that is overlaid onto the deformed model to guide the manual planning of bone reposition.

Over the last few decades, a lot of systems have been develop for CMF surgery. Most of these systems focus on predicting post-operative facial appearance to assist the surgeon in evaluating the plan as well as facilitate the communication between the surgeon and the patient [KGA*96, KGPG96, KGRG98, KRG*99, TGG99, CP00, XIS*00, XSC*00, GZDH01, CMPB02, GZDH03, MSCS03, CMC*04, GIR04, MSCP04, SBF*04, SVBBC09]. In addition to predicting face appearance, the system of Gladilin, Zachow et al. [GZDH03] also predicts post-operative facial expressions. Some systems generate reconstructed models of the patient from the deformed ones [LCL*03, ZLES05, DMCP*06, CSP*07, CTS*10]. Commercial systems such as Brainlab [GWL99a] and SurgiCase CMF [Mim] also provide partial reconstruction based on symmetry. Few other systems perform restoration of mandible using fracture surface matching [BCT*04, CBRY06, CBRY07]. To the best of the author's knowledge, there is no existing predictive system that generates restored skull model from deformed skull model.

3.3 Summary

Existing restoration and reconstruction methods are summarized in Table 3.1. Manual manipulation methods display 3D model of the patient's skull in the computer monitor and allow the surgeon to virtually cut and reposition the bones in the 3D model to generate restored model. They are relatively easy to implement, and give the surgeon maximum control over how the bones in the deformed model should be repositioned. As a result, bone repositioning is planned by the surgeon manually, which can be very tedious and time-consuming.

Reconstruction methods generate reconstructed model to estimate the normal model based on the correlation between the healthy parts and the fractured parts. Symmetry-based methods reflect the healhty parts of a deformed model about the lateral symmetry plane and use the reflected parts as estimates of the normal shapes of the fractured parts. They do not require any reference model. But they require the presence of healthy symmetric parts to reconstruct the fracture parts on the opposite side of the skull. When both sides of the skull are fractured, which is common in impact injuries, these methods cannot be applied. Geometric reconstruction methods register a reference model to the healthy parts of a deformed model and use the registered reference model to estimate the normal shapes of the fractured parts. These methods do not require the presence of healthy symmetric parts. Instead, they use a single reference model to generate the reconstructed model. Their reconstruction accuracy depends on the similarity between the reference model and the normal model, and the strength of the correlation between the healthy parts and deformed parts. Statistical reconstruction methods overcome the limitation of geometric reconstruction by matching a statistical reference model to the healthy parts of a deformed model and uses the matched statistical model to infer the fractured parts of the deformed model. They require a statistical model, the construction of which requires a large amount of training samples of healthy skull models. Their reconstruction accuracy depends on how well the statistical model captures the normal shape variation of the patients' normal model. In the case that such normal shape variation is not adequately captured, then only the mean shape of the statistical reference can be used. The. statistical reconstruction becomes geometric reconstruction.

Moreover, similar to geometric reconstruction methods, statistical reconstruction methods relies on the correlation between the healthy parts and the deformed parts.

Fracture surface matching methods reposition fractured bones by determining their correct relative positions and orientations based on shape complementarity of adjacent fracture surfaces. They do not require any reference models or the presence of healthy parts in the deformed model. Instead, they produce the restored model by computing the correct positions and orientations of the fractured bone fragments. However, they require the features of fracture surfaces to be well captured in the deformed model. In the case of impact injuries, where the fracture surfaces abrade each other, fracture surface matching methods become inaccurate.

Many computer-aided systems have been developed for CMF planning. Reactive systems are real-time systems that attempt to simulate the reactions of the body in response to user inputs. They are more suitable for surgery training than surgery planning. Predictive systems attempt to accurately predict surgical results of complex surgical procedures based on predefined or user-specified surgical requirements. They are suitable for planning complex CMF surgery. Most of them generate post-operative facial appearance, while a few of them also generate facial expressions. Some systems generate reconstructed model that can be used to guide manual planning. Several systems can generate surgery plan for mandible restoration.

In conclusion, there is no existing predictive system that assists a surgeon to easily generate surgery plan for CMF surgery on the skull, and there is no automatic, reliable and accurate method for generating the restored model of a patient's skull from his/her deformed model. These are the focus of this thesis proposal.

Table 3.1: Comparison of Restoration & Reconstruction Methods.

Method	Citations	Approach	Bone repositioning	Reference model	Need healthy parts	
					Symmetric	Non-symmetric
Manual manipulation	[KGA*96, KGPG96, KGRG98, GEH*99, GWL99a, KRG*99, TGG99, CP00, BPM*00, XIS*00, XSC*00, GZDH01, CMPB02, TPS*02, GZDH03, LCL*03, MSCS03, CMC*04, GIR04, MSCP04, SBF*04, XGT05, ZLES05, DMCP*06, CSP*07, KSS09, SVBBC09, CTS*10, Mim]	Restoration	Yes	No	No	No
Symmetry-based reconstruction	[GWL99a, LCL*03, DMCP*06, CSP*07, CTS*10, WYLL11, Mim]	Partial reconstruction	No	No	Yes	NA
Geometric reconstruction	[GMBW04, BSMG09, WYLL11]	Reconstruction	No	Single	No	Yes
Statistical reconstruction	[Phi05, ZLES05, BSMG09, LAV09]	Reconstruction	No	Statistical	No	Yes
Fracture surface matching	[BCT*04, CBRY06, CBRY07]	Restoration	Yes	No	No	No
Proposed		Restoration	Yes	Single or statistical	No	Yes

Chapter 4

Proposed Thesis Project

The review in Chapter 3 shows a gap in existing work on CMF surgery planning. This gap leads to the proposed research topic which consists of two main objectives:

- Development of a computer-aided procedure for assisting a surgeon in deriving a CMF surgery plan (Section 4.1).
- Development of a method for generating the restored model from a patient's deformed model of the skull (Section 4.2).

4.1 CMF Surgery Planning Procedure

The proposed computer-aided CMF surgery planning procedure takes CT or MRI (Figure 4.1) of a patient's skull as input and generates the surgery plan for restoring the skull. It consists of three main stages:

1. Segmentation and construction of 3D deformed model (Section 4.1.1).
2. Identification of midline landmarks and fixed bone fragments (Section 4.1.2).
3. Restoration of deformed model (Section 4.2).

In the first stage of the procedure, the 3D computer model called deformed model is constructed from the input images. The deformed model contains separate 3D meshes for the bone fragments in the deformed skull. This is used for the simulation of bone repositioning. The construction of the deformed model requires segmentation and 3D mesh generation. The segmentation method identifies the regions in the medical images that correspond to the bone fragments (Section 4.1.1). Then, the 3D mesh generation algorithm constructs the surface mesh for each of the bone fragments from the segmentation result.

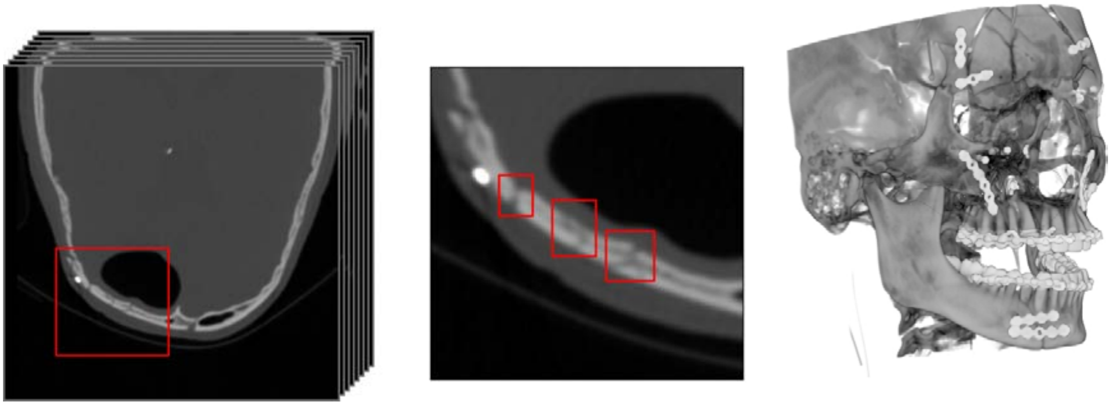

(a) (b) (c)

Figure 4.1: CT images of a patient's skull. (a) CT slices. (b) Zoom-in view, red regions are fractured. (c) Volume rendering of the images.

The second stage (Section 4.1.2) acquires inputs corresponding to the user's requirements of the surgery. These requirements include midline landmarks that should fall on an approximate symmetric plane of the skull and the undeformed bone fragments that should not be repositioned in the surgery.

The last stage of the CMF planning procedure applies a restoration algorithm to generate the restored model from the deformed model based on the requirements acquired in the second stage. Detailed description is presented in Section 4.2.

4.1.1 Segmentation and Construction of 3D Deformed Model

Some existing methods have the potential to solve segmentation problem in the proposed application. Thresholding algorithm [SS04] is suitable for skull segmentation (Figure 4.2) because voxel intensities of the bony structures are higher than those of other regions. However, in our application, we need a separate mesh model for each of the bone fragments in the deformed model. Thresholding algorithm does not provide any information about which voxel belongs to which bone fragment. Therefore, though thresholding algorithm is suitable for segmentation of bones in general, it is insufficient for segmenting separate bone fragments.

Fully automatic segmentation of individual bone fragments from CT images is a very challenging problem. State-of-the-art commercial segmentation software such as Amira [Gmb] provides only a thresholding algorithm for automatic segmentation, which is insufficient as discussed earlier. ITK-SNAP [YPH*06], an open-source segmentation software, provides a snake algorithm [KWT88] for automatic segmentation. The snake may leak

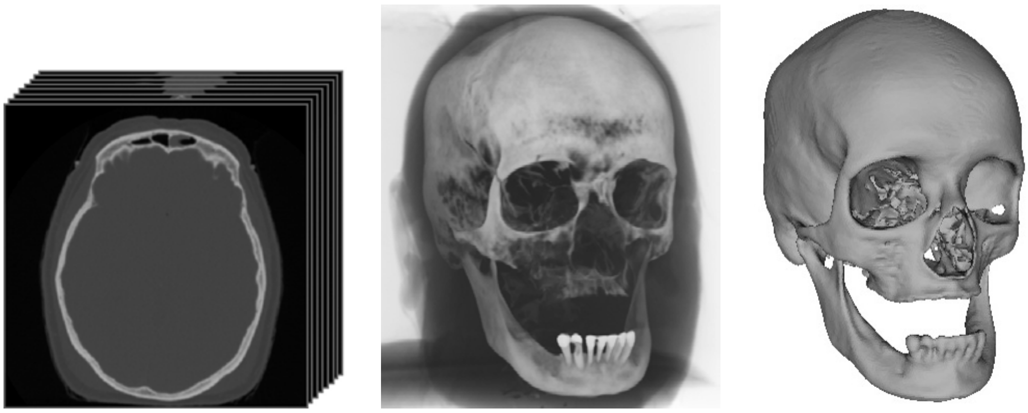

(a) (b) (c)

Figure 4.2: Threshold segmentation. (a) CT images. (b) Volume Rendering. (c) Skull model constructed from threshold segmentation result.

into irrelevant regions such as the cracked regions between bone fragments and the regions belonging to neighboring bone fragments. There is no existing fully automatic method that can segment separate bone fragments. The focus of the proposed research is CMF surgery planning and restoration of deformed skull models. Fully automatic segmentation of separate bone fragments is outside the scope of this research.

In the proposed procedure, bone fragment segmentation is performed in a semi-automatic manner. First, we apply the thresholding algorithm to segment the whole skull from the CT images. Usually, parts of the fractured regions are segmented because they also have high intensities. Then, we manually mark the fractured regions using the interactive segmentation tool provided by ITK-SNAP [YPH*06]. Deformed model rendering, volume rendering and CT slices are used to guide this marking step. After that, we identify the continuous bone regions in the segmentation result as separate bone fragment regions. Finally, we apply the marching cubes algorithm [LC87] to generate meshes from the bone fragment regions. Figure 4.3(c) shows the generated mesh model for the right cheek bone fragment.

For comparison with our method, we applied a combination of thresholding and snake algorithm to segment a bone fragment of the right cheek bone. First, we applied the thresholding algorithm to generate the initial snake. Then, we ran the snake algorithm to segment the bone fragment. Finally, we use marching cubes algorithm to generate the mesh. Figure 4.3(a) shows that the snake algorithm leaked through the crack regions to the neighboring bone fragments because the cracks between the bone fragments were very small and unclear in the images.

We further verified the correctness of the constructed deformed model (Figure 4.4(a)). One deformed model was verified by an experienced CMF surgeon in NUH who operated

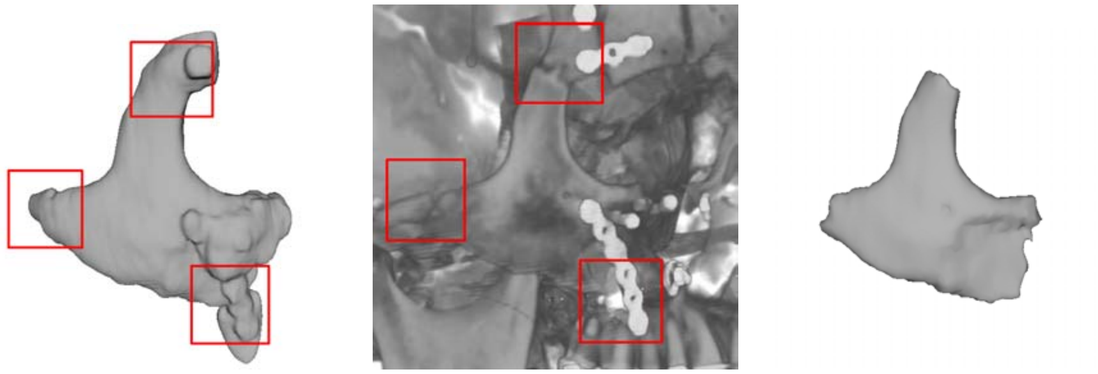

(a) (b) (c)

Figure 4.3: Snake segmentation. (a) 3D mesh constructed from snake segmentation result shows that the snake leaks into neighboring regions (square box). (b) Volume rendering. (c) Correct 3D mesh without leakage.

on the patient. Volume rendering (Figure 4.4(b)) and CT images (Figure 4.4(c)) were provided to assist in the verification. The surgeon concluded that the deformed model was correctly segmented.

4.1.2 Identification of Midline Landmarks and Fixed Bone Fragments

Midline landmarks of normal skulls and skulls with minor injury can be identified by the automatic algorithm to be presented in Section 5.2. It registers the reference model with known landmarks to a target skull to locate the landmarks on the target skull. Then, it iteratively refines the landmarks' locations according to their medical definitions.

For patients with severe head injuries, their skulls may be grossly distorted. The landmarks may not be located at their normal positions because the bone fragments are displaced. Thus, the proposed automatic algorithm may fail for these cases. In the current implementation, the surgeon is asked to indicate the midline landmarks on the bone fragments of the deformed model. A graphical user interface is provided for manual indication of midline landmarks (Figure 4.5). It renders the deformed model and provides the user the flexibility to view the model in different angles. The user can simply right click on the corresponding position on the model to locate the landmarks. The GUI also allows the user to indicate the fixed bone fragments that should not be repositioned and the movable bone fragments that can be repositioned in the surgery (Figre 4.5).

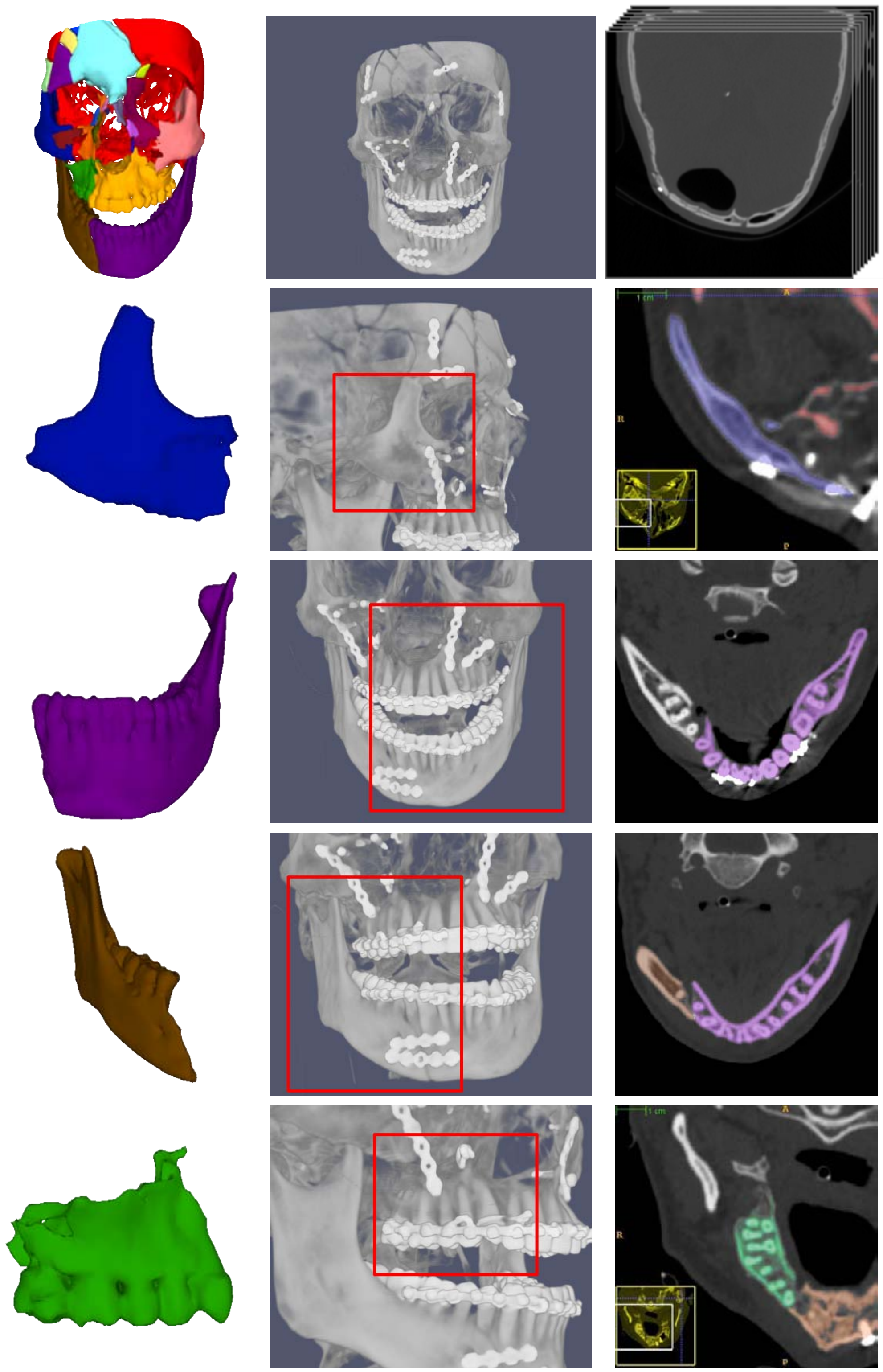

(a) (b) (c)

Figure 4.4: Segmentation and 3D deformed model construction result. (a) Surface model. (b) Volume rendering. (c) CT slice. (Row 1) Entire skull. (Row 2) Right cheek bone. (Row 3) Left lower jaw. (Row 4) Right lower jaw. (Row 5) Right upper jaw.

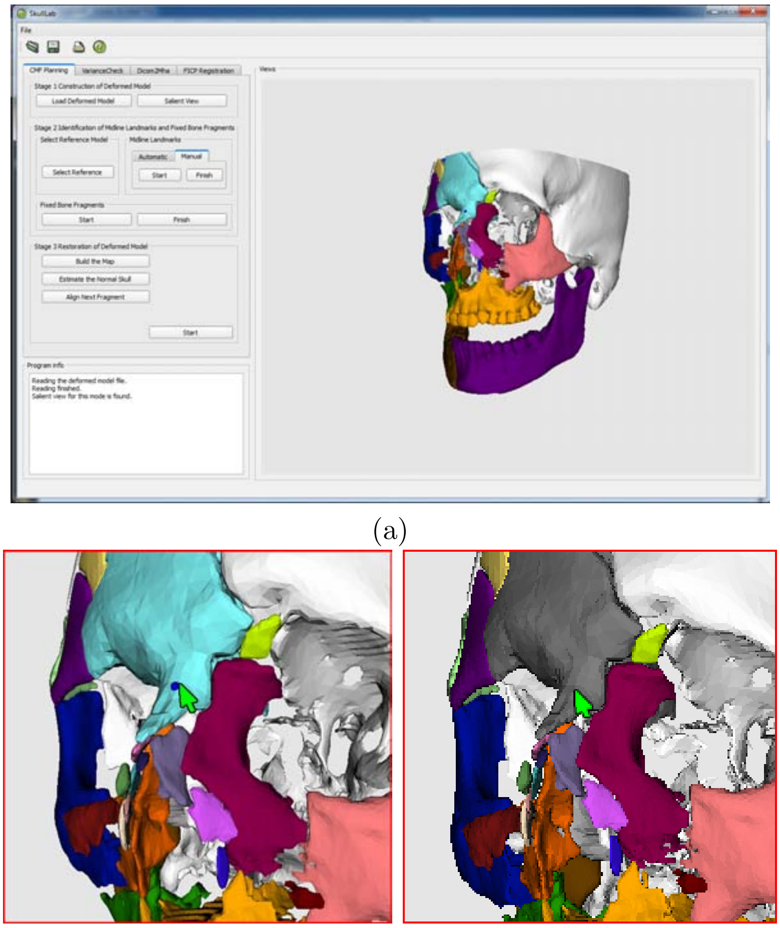

(a)

(b) (c)

Figure 4.5: Graphical user interface for identification of midline landmarks and fixed bone fragments. (a) GUI. (b) Identification of midline landmarks. (c) Identification of fixed bones.

4.2 Restoration of Deformed Model

To develop an accurate and efficient algorithm for restoration of a deformed model, it is necessary to first discuss the inputs (Section 4.2.1) and identify the principles that guide the algorithm (Section 4.2.2). Then it will be clear how and why the algorithm works (Section 4.2.3).

4.2.1 Inputs

The inputs of the problem include the following:

- Deformed Model D.
  The deformed model D contains bone fragment models B_k. These bone fragments are divided into a set of fixed bone fragments and a set of movable bone fragments. Each bone fragment model is a closed mesh containing a set of vertices.
- Reference Model F.
  The reference model F is a closed mesh model of the normal reference skull. F has an approximately symmetric plane P_F.
- Midline landmark set L.
  The midline landmark set L consists of six midline landmarks $l_1, l_2, ..., l_6$, which are located on the bone fragments in the deformed model.

4.2.2 Principles

The output of the algorithm is the restored model R which represents the patient specific model after applying repositioning operations to the bone fragments B_k in the deformed model D. The desired output R has the following characteristics, which describe the requirements of the problem:

1. No Collision.
   There should be no collision between any two bone fragments (Figure 4.6) because physical bones do not penetrate each other.
2. Symmetry.
   The left and right side of the restored model should be as symmetric to each other as possible with respect to a symmetric plane. Although there is significant asymmetry in the human skull [RRS03, Woo31], in real surgeries, due to the lack of other information about the patient's normal model prior to injury, the surgeon usually tries to make the skull as symmetric as possible.

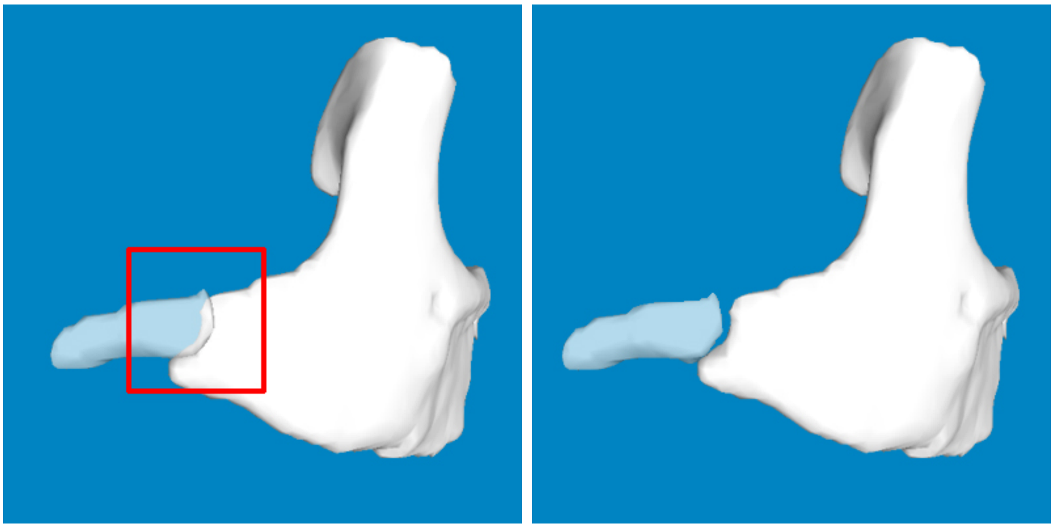

(a) (b)

Figure 4.6: No collision principle. (a) With collision. (b) Without collision.

3. Midline.
   In the restored model R, the midline landmarks should lie on the symmetric plane of the skull. This is because, in normal anatomy, the symmetric plane of a skull passes the midline of the skull.

4. Normality.
   The restored model should look like a normal person's skull. It is noted that there is a wide variation of normal look among people in different age, gender and racial groups.

5. Joint Continuity.
   The surfaces of two neighboring bone fragments should be continuous across the joint.

We propose to follow four principles to solve the complex restoration problem. These principles are symmetry principle, midline principle, normality principle, and ordering principle.

1. Symmetry Principle

Symmetry principle aims at restoring the deformed model D to a state R such that the left and right side of the restored model R is as symmetric to each other as possible with respect to a symmetric plane. The symmetric plane of the patient's deformed model does not exist because the patient's skull is distorted due to fracture, and the bone fragments that contain the midline landmarks that determine the symmetric plane are displaced. On the other hand, symmetric plane P_F of the reference model F fits the symmetry principle. Thus, if we align the reference model with the patient's model, the symmetric plane P_F can be used to guide the restoration of the symmetry of the patient's model. With an ideal solution, the symmetric plane P_R of R would coincide with the symmetric plane P_F of F.

2. Midline Principle

The midline landmarks in the restored model R should lie on the symmetric plane of the skull. Initially, the principle can be checked against P_F. As the algorithm converges toward a good solution, P_R can be computed and it should be close to P_F. Then, this principle can be checked against either P_R or P_F.

3. Normality Principle

Normality principle requires that the restored model R should look normal. We first show two experiments that were conducted to examine the characteristics of normal skull models. Then we provide the normality principle based on the observations found in the experiments.

Experiment A

We first conducted an experiment to compare the normal skull models of different people. In this experiment, four healthy skull models were used. One of the models was selected as a reference. The other three models were aligned with the reference model using the Fractional Iterative Closest Point algorithm (FICP) [PLT07]. FICP is a variant of ICP which is robust to the natural variation between the skulls. Like ICP, FICP iteratively computes the best rigid transformation that registers the reference to the target. The difference is that in each iteration, FICP computes the transformation using only a subset of mesh points on the reference model whose distances to the target model are the smallest. After alignment, the differences from the vertices of the reference model to their closet points on the surface of the aligned target models were calculated.

We show the differences at the vertices of the reference model using pseudo color (Figure 4.7). The warmer the color, the larger is the difference. Figure 4.7 shows that the difference between the normal skull models and the reference model is large in most regions. The mean differences of the three pairs are also large in general.

The experimental result shows that the mean difference of the skull has an average of 1.67 mm with a standard deviation 1.52. This value is large compared to the resolution

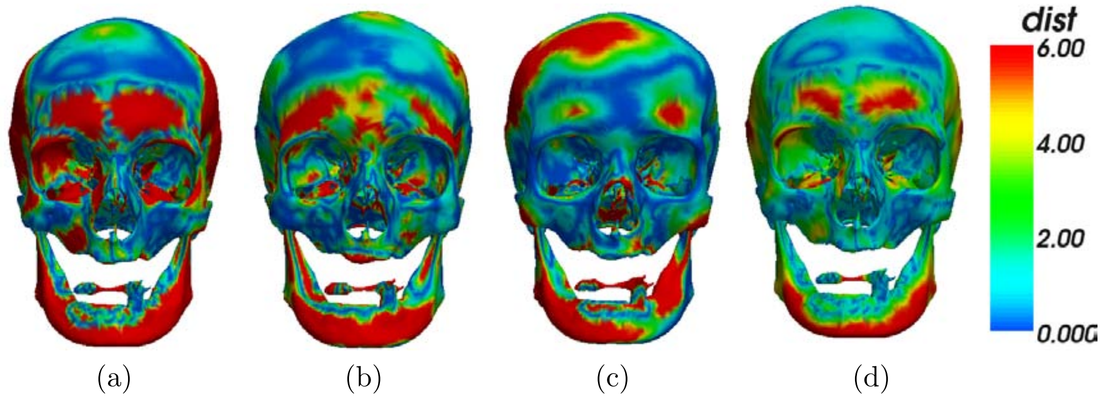

Figure 4.7: Difference between normal skull models and a reference model. (a) MANIX vs. Adam. (b) MANIX vs. BWH. (c) MANIX vs. Eve. (d) Mean.

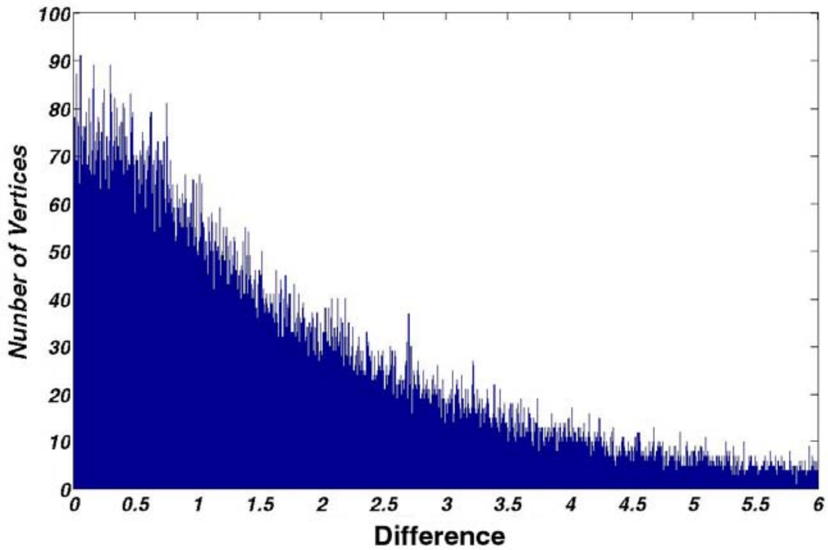

Figure 4.8: Distribution of mean difference.

of the CTs, which is around 0.5 mm. The distribution of the mean difference (Figure 4.8) shows that the mean difference is large in most regions. Therefore, any single normal skull model cannot be directly used to represent the normal anatomy of another person.

Experiment B

We conducted another experiment to examine the local variation of difference. The local variation of difference is defined as the variation between the difference at a vertex of the reference model and the mean difference at its neighboring vertices. It is small if the skulls vary from each other similarly in a local region and large if the skulls vary from each other differently in a local region.

The result shows that the local variation of difference averaged over the test models

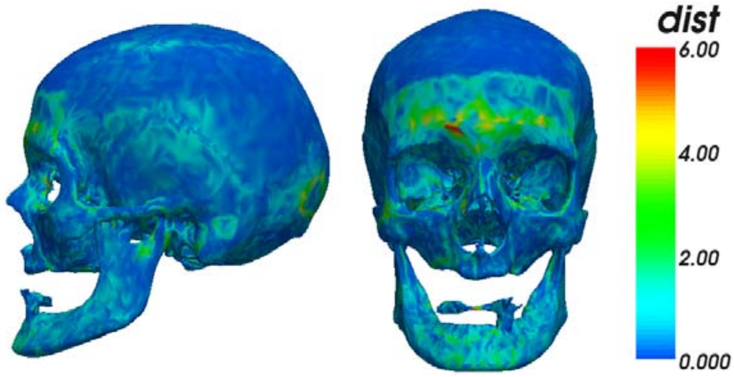

(a) (b)

Figure 4.9: Mean local variation of difference. (a) Side view. (b) Front view.

has an average of 0.46 mm with a standard deviation 0.65. Figure 4.9 shows that the mean local variation of difference in most regions of the skull is relatively small compared to the mean difference (Figure 4.7(d)). The distribution of the mean local variation of difference (Figure 4.10) shows that the mean local variance of difference is smaller than the CT resolution of 0.5 mm at most vertices.

Principle

The normality principle is based on the observations from the previous experiments. This principle requires that, if a model is normal, the local variation of difference is small. Figure 4.11 illustrates the idea of applying the normality principle. Figure 4.11(a) shows the deformed model. We are confident of the blue parts which are the fixed bones, and we are going to reposition the green parts which are the fractured bone fragments. We first align a normal reference model (red) to the deformed model. We then compute the differences (Figure 4.11(b)) in the confident region (blue part).

If we directly propagate the differences at boundary vertices of confident region to the vertices in the nearby regions, we may get the shape indicated by the green line (Figure 4.11(c)). Locally, it is like a displaced reference model, and globally it is like a scaled version of the reference model. However, we are uncertain about this shape because the **Experiment B** shows that there is a small local variance of differences.

We should allow for a small amount of local variation of differences. The amount of allowed variation, i.e. uncertainty in the actual positions, can be estimated as the mean change of variance value plus one standard deviation (1.11), which captures 95.7% of normal cases. By allowing the local variation of difference, we can have a range of the possible normal position for the nearby vertices. This range becomes larger when the vertices are far away from the confident regions because the uncertainty accumulates over

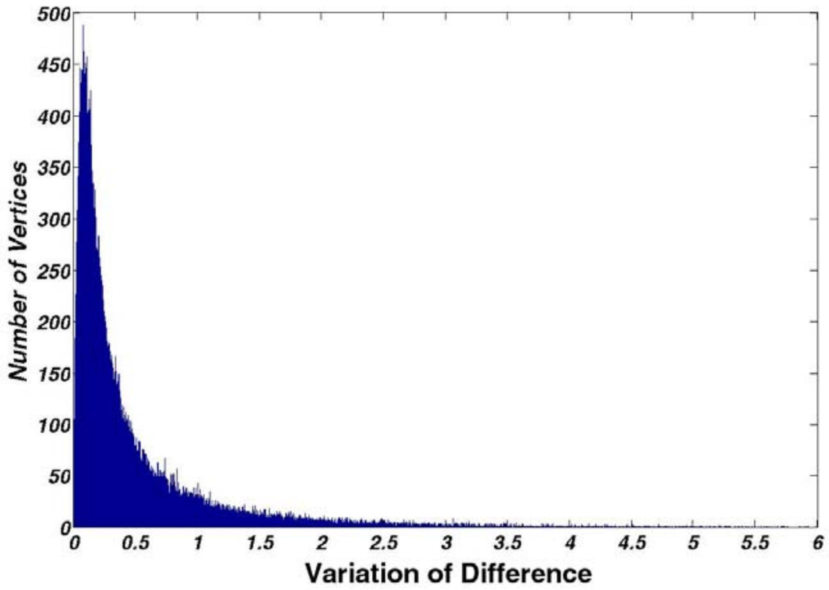

Figure 4.10: Mean variation of difference distribution.

distance.

We can also consider the joint continuity at the boundary of confident region. The joint continuity requires that an immediate neighboring vertex of confident region should have the same difference as its neighboring confident vertices. Thus, we have a stronger constraint to the immediate neighboring vertices of confident region. This constraint gives rise to the shape of the uncertainty region shown in Figure 4.11(f). Any bone fragment that completely fall in the uncertainty region can be considered to be normal.

This normality check scheme can further be extended when more normal skull models are available. In that case, we can estimate the distribution of the differences at each vertex. Thus, we can measure the possibility of having a pose of a bone fragment by multiplying the possibility of having the differences at all the vertices that forms that pose.

4. Ordering Principle

The ordering principle of the restoration algorithm is to always use the bone fragments whose poses we are confident of to help determine the optimal poses of the nearby bone fragments whose current poses we are less confident of. Figure 4.12 illustrates the ordering principle. We are confident of the blue region, and the bone fragments B_1, B_2 and B_3 are unconfident ones. If we use the pose of B_1 to help determine the pose of B_2, we may get the result shown in Figure 4.12(b). In this case, we are less certain about the new pose

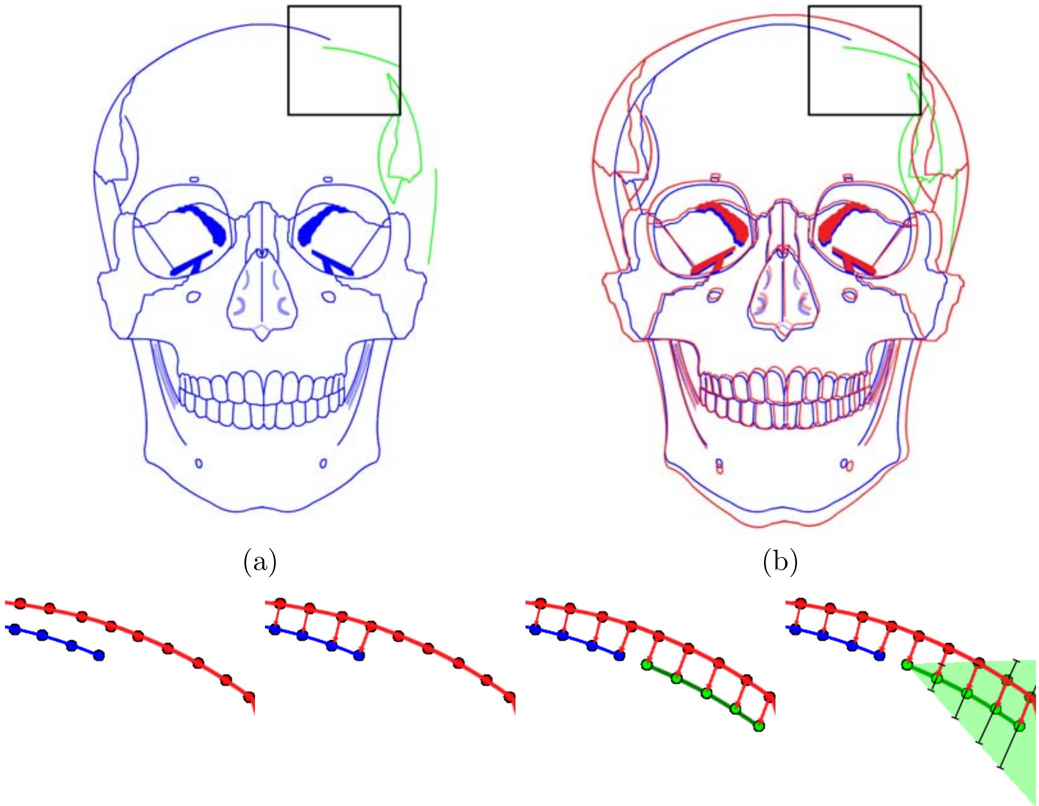

(a) (b)

(c) (d) (e) (f)

Figure 4.11: Normality principle. (a) Deformed model. Blue parts are fixed bone fragments and green parts are bone fragments to be repositioned. (b) Reference model (red) aligned to deformed model. (c) Zoomed view of rectangular region of (b). (d) Differences in the confident region. (e) Positions (green) estimated by constant difference. (f) Positions (green) estimated allowing variations of difference which accumulates to from the uncertainty region (green).

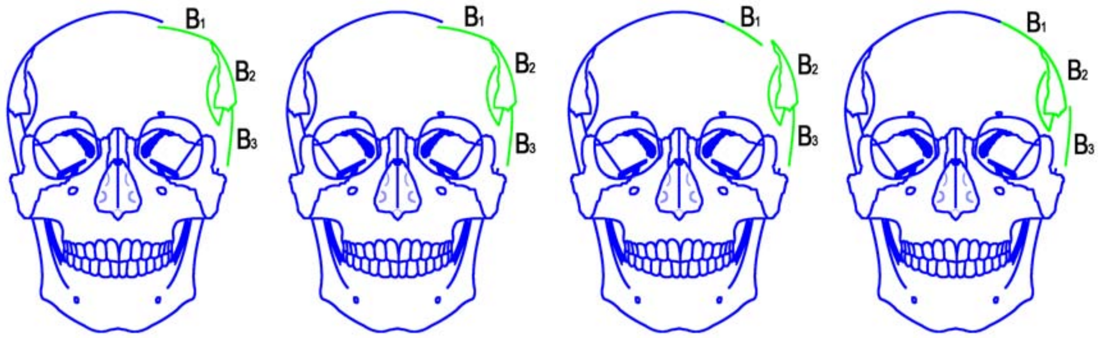

(a) (b) (c) (d)

Figure 4.12: Ordering principle. (a) Deformed model. (b) Reposition B_2 using the unconfident pose of B_1. (c) Reposition B_1 using the confident region. (d) Reposition B_2 after (c) using the confident region plus the new pose of B_1.

of B_2 even though the repositioning algorithm is correct. The resulting new pose of B_2 is less likely to be correct. In contrast, we can first reposition the pose of B_1 guided by the shape of its nearby confident region (Figure 4.12(c)). If the repositioning algorithm gives good pose of B_1 that best follows the other principles (i.e., no collision, symmetry, midline and normality), we are confident of the new pose of B_1. Then the new pose of B_1 can be used to guide the repositioning of B_2 (Figure 4.12(d)). Again, if the repositioning algorithm gives good result, we are more confident about the new pose of B_2. Overall, it is better to use only the confident region to guide the repositioning of unconfident bone fragments. Among the unconfident bone fragments, we should select an unconfident bone fragment that is adjacent to confident region because the normality principle provides tighter constraint to the neighboring bone fragments. There might be several unconfident bone fragments that are adjacent to confident regions. In this case, we can choose an arbitrary one or the largest one.

4.2.3 Restoration Algorithm

Now we can provide an overview of the restoration algorithm. The algorithm starts with the patient's deformed model. First, it aligns the reference model to the deformed model to guide the restorations. Then, it follows the ordering principle to select an unconfident bone and apply a single bone fragment repositioning algorithm to reposition it. The repositioning algorithm finds the new pose that best meets the symmetry, midline and normality principles. This is repeated for each unconfident bone fragment. After one iteration of repositioning all the unconfident bone fragments, the deformed mode becomes an approximately restored model which is better than the deformed model in terms of symmetry, midline, normality and joint continuity. Then, the restoration algorithm aligns the reference model to the restored model and obtains more accurate symmetric plane estimation, and the reposition of bones is repeated. This process is iterated until the change of bone fragments' poses is small enough.

Initially, the restored model has large errors, in terms of symmetry, midline and normality. The repositioning of the bone fragments in the manner described above seeks to reduces these errors in a controlled manner. As the algorithm iterates, the errors are expected to reduce further until a near optimal solution is obtained when the algorithm converges.

The restoration algorithm is summarized as follows:

Algorithm 1: Skull Restoration Algorithm

Input: Reference model F, patient's deformed model D, midline landmarks L.

Output: Patient's restored model R.

1. Initialize $R \leftarrow D$.
2. Repeat until convergence:
   (a) Align the reference model F to R.
   (b) Mark fixed bone fragments as confident and movable bone fragments as unconfident.
   (c) For each unconfident bone B in decreasing order:
      i. Apply Monte Carlo algorithm to reposition B according to the principles of no collision, symmetry, midline, and normality.
      ii. Mark B as confident bone.

The main idea of the Monte Carlo algorithm is to generate new random poses of the bone fragments and select the optimal pose that meet the principles and minimizes a restoration error E which consist of two terms: symmetry error and midline error.

The symmetry error is measured by the asymmetry $d_s(v_i, m(v_i), P_F)$ between the vertices v_i in B and their symmetric corresponding point $m(v_i)$ on a confident bone with respect to the plane P_F:

$$E_S = \sum_{v_i \in B} d_s^2(v_i', m(v_i'), P_F) \tag{4.1}$$

If v_i has no symmetric correspondence on a confident bone, it is not included in the computation of E_S. The symmetry principle is met by minimizing E_S.

The midline error E_M is measured by the distances $d_m(l_i, P_F)$ from the midline landmarks l_i on B to the symmetric plane P_F:

$$E_M = \sum_{l_i \in B} d_m^2(l_i, P_F) \tag{4.2}$$

The midline principle is met by minimizing E_M.

The restoration error E is defined as:

$$E = \lambda_S E_S + \lambda_M E_M \tag{4.3}$$

where the λ_S and λ_M are the parameters to balance the effect of the two error terms. By minimizing E, both symmetry principle and midline principle are met.

Metropolis criterion [MRR*53] helps the Monte Carlo algorithm to escape from local minimals and reach global minimal. It favors decreases in E and always accepts a new pose with lower error than the previous pose. On the other hand, Metropolis criterion also allows increase in the error with a probability p controlled by a temperature parameter t which increases over iterations and the difference of error ΔE:

$$p = e^{-\alpha t \Delta E} \tag{4.4}$$

where α is a constant that controls the acceptance rate. The temperature parameter t starts with a small value which has high probability of accepting a new pose with increased error. This helps the algorithm to jump out of local minimals. As the algorithm iterates, t increases to a higher value which has a lower probability of accepting a new pose with increased error. Thus the algorithm will converge to the nearby local minimal. Though the Monte Carlo algorithm is likely to reach global minimal, it might still reach local minimals. To avoid the local minimums, we run the Monte Carlo algorithm multiple times to produce a set of candidate poses for the bone fragment and select the one with minimal restoration error as the final result. The Monte Carlo algorithm is summarized as follows:

Algorithm 2: Monte Carlo Bone Repositioning Algorithm

Input: Reference model F, patient's (partially) restored model R, bone fragment B to be repositioned.

Output: Patient's restored model R with bone fragment B repositioned.

1. Repeat for a fixed number of iterations:
   (a) If B does not collide with adjacent confident bone fragments, and
   B falls completely in the uncertainty region, then
      i. Compute restoration error E according to symmetry and midline principles.
      ii. If restoration error E is accepted by Metropolis criterion,
      then accept B's pose;
      else reject B's pose and revert to the previous pose.

The single bone repositioning algorithm gives one best pose for each bone fragment considering the restoration error E. It might miss a good restoration plan that is optimal when considering the overall shape while sub-optimal when considering some bone fragments. To avoid missing this kind of sub-optimal poses, we can extend our algorithm by always keeping the best n candidate poses for a bone fragment when considering all the poses of previous bone fragments. Then from each of them we generate n best candidate poses for the next bone fragment and again keep only n best ones. We iterate this procedure for all the bone fragments. After that, we have n candidate poses for the final bone fragment. These n candidate poses together with all the poses of previous bone fragments that leads to them form n candidate restored models. Finally, we can measure an overall restoration error which is the sum of the restoration error for all the movable bones and choose the restored model with lowest overall restoration error.

4.3 Research Schedule

The tasks involved in completing the proposed research can be summarized as follows:

- Automatic midline landmark identification (done).

- Manual midline landmark indication and fixed bone fragment indication user interface (done).
- Robust alignment algorithm (done).
- Collision detection algorithm (not done).
- Normality checking algorithm (not done).
- Monte Carlo bone fragment repositioning algorithm (not done).
- Validation (not done).

Some of the tasks have already been accomplished, and the will be presented in Chapter 5. The remaining tasks will be completed according to the following schedule:

- Present - July 2012: Collision detection algorithm.
- August 2012: Normality check algorithm.
- September 2012: Monte Carlo bone fragment repositioning algorithm.
- October 2012: Overall framework.
- November 2012 - March 2013: Validation and thesis writing.

Chapter 5

Preliminary Work

Preliminary work has been done on robust registration (Section 5.1) and MSP and FP identification (Section 5.2). They are presented in the following sections.

5.1 FICP Registration

A robust registration algorithm is need in the proposed project. In real applications, models to be registered may vary greatly in size, shape details and completeness. To achieve good registration under these conditions, Fractional Iterative Closest Point (FICP) [PLT07], a variant of ICP [BM92] which is robust to these variations, is selected. Like ICP algorithm, FICP iteratively computes the best similarity transformation that registers the template to the target. The difference is that in each iteration, FICP computes the transformation using only a subset of template points whose distances to the target model are the smallest.

FICP minimizes a fractional root-mean-square distance:

$$E = \frac{|V|}{|D|}^{\lambda} \sqrt{\frac{1}{|D|} \sum_{x_i \in D} \|T(x_i) - f(T(x_i))\|^2} \tag{5.1}$$

where V is the set of template points, D is a subset of V with correspondence, f is the closest point function, T is the transformation to be optimized, and λ is a constant parameter. In current implementation, similarity transformation is used for T to cater to size difference between the models to be registered, and λ is set to 2.7 empirically.

The algorithm to solve this problem is to iteratively optimize the E. It does the following two steps in each iteration until the termination criteria satisfies:

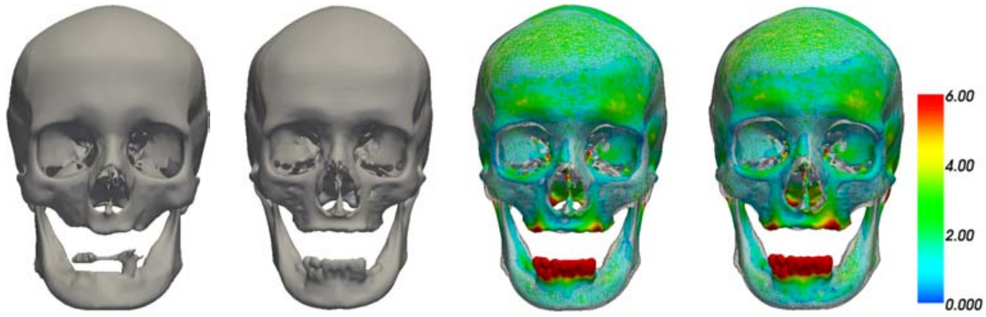

(a) Source (b) Target (c) ICP result (d) FICP result

Figure 5.1: Comparison of FICP and ICP on registering similar models.

1. Find the set D that minimizes E
2. Compute transformation T for the vertices in D

The FICP algorithm first selected a set of the vertices D in the template by optimizing the objective function. As can be seen, for target model with n vertices, there are 2^n possible subsets, which is a huge search space. Based on the observation that, for the same T, in all the subsets with the same size m, the subset that contains the first m points with closet distance to the target model has the smallest E value. Therefore, the algorithm only need to compare n this kind of subsets and find the one with smallest object value.

With given set of points with correspondence, the next step in is to find the best transformation to align them. This is a well solved problem. The algorithms to find the transformation can be found in [JKS95, Har97]. It composites of four main steps:

1. Remove the translation by moving object's centroid to origin of coordinate system.
2. Determine scaling factor by comparing mean vector length.
3. Compute rotation matrix.
4. Compute the translation with the computed scaling factor and rotation matrix.

We compared the FICP with traditional ICP algorithm on real skull models. Experiments are conducted registration of similar models and models with large variance. Figure 5.1 (a) and (b) show two similar models to be registered in the first experiment. The registration result shown in Figure 5.1(c) and (d) indicate that both ICP and FICP can find good registration result for them. Figure 5.2(a) and (b) show two models with large variance to be registered in the second experiment. Figure 5.2(c) and (d) show the

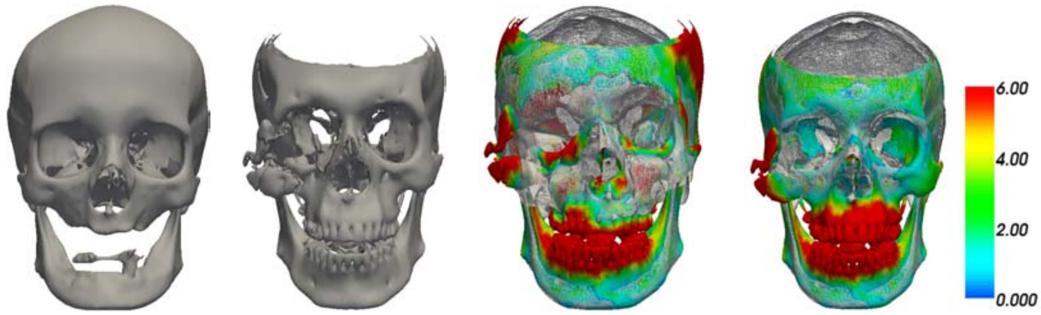

(a) Source (b) Target (c) ICP result (d) FICP result

Figure 5.2: Comparison of FICP and ICP on registering models with large variance.

results of ICP and FICP algorithms respectively. As can be seen, ICP which is sensitive to the outliers resulted in bad registration result (Figure 5.2(c)), while FICP which is more robust to variance between models still gave good registration result (Figure 5.2(d)).

5.2 FP, MSP and Midline Landmark Identification

In anatomy, FP and MSP are defined by the midline landmarks on them. They are used to define the skull's anatomical orientations (Figure 2.2). These orientations, in turn, are used to define craniometric landmarks. For example, the orbitale is the lowest point of the orbit. But the lowest point changes as the orbit is rotated. Therefore, to accurately identify FP, MSP and midline landmarks, an iterative algorithm is required to iteratively refine the estimations of the landmarks, MSP and FP. Moreover, a good initialization of the algorithm is required to yield optimal solutions.

In this section, we present a method to automatically identify the FP, MSP and midline landmarks robustly and accurately [CLL11]. It registers a template skull model with known landmarks to a target skull using the FICP registration discussed in Section 5.1 to initially locate the landmarks, FP, and MSP on the target skull. Then, it iteratively refines the landmark locations, then FP and MSP according to their medical definitions. Test results show that the proposed algorithm is more robust and accurate than symmetry-based methods. Moreover, it can also be applied to partial skull models of real patients.

An overview of the iterative algorithm is given below:

Algorithm 3: FP, MSP and Midline Landmarks Identification Algorithm

Input: Template mesh model, target mesh model.

Output: The FP, MSP and midline landmarks on the target mesh model.

1. Register a template mesh model with known landmarks to the target mesh model. This step uses the FICP algorithm discussed in Section 5.1.
2. Locate the landmarks on the target model using the registered template model, and fit FP and MSP to the landmarks in least square manner. These landmarks and the fitted planes serve as the initial estimates.
3. Repeat until convergence:
   (a) Refine locations of FP landmarks according to their medical definitions, and fit FP to the refined FP landmarks.
   (b) Refine locations of MSP landmarks according to their medical definitions, and fit MSP to the refined MSP landmarks, keeping it orthogonal to FP.

Experiments were conducted to validate the proposed method. Four full skulls were used in the experiments, of which three were from Visible Human Project, and one was from OsiriX. One full skull which is shown in Figure 2.2 was used as the template and the others were the test targets. In clinical practice, CT images are acquired only for the parts of the skulls under treatment. For this reason, the 3 target full skulls were cut at the top and the bottom to produce 3 additional partial skulls for testing. The only requirement was that all the FP and MSP landmarks could still be located on the partial skulls. Moreover, three partial skulls of patients from a local hospital were also used for testing. With this setting, there are three groups of targets, namely, full skull, partial skull (generated from the full skull), and patient skull.

The resolutions of the CT images of the skull models ranged from 0.47 to 1 mm/pixel. The CT images were segmented and 3D mesh models were reconstructed from them.

The proposed algorithm was applied to the test targets. For comparison, an automatic algorithm that estimated MSP based on symmetry was also implemented and tested. For fair assessment, the same initialization was performed before executing the symmetry-based algorithm.

To assess the accuracy of the algorithms, a human expert was asked to mark ground-truth landmark points on the skulls. Their mean distances to the detected planes were

Table 5.1: Comparison of mean error. (full) Full test skulls. (partial) Partial skulls cut from full skulls. (patient) Patients' partial skull models. (ini) Initialization. (sym) The symmetry-based method. (prop) The proposed method.

skull	FP (mm)		MSP (mm)		
type	ini	prop	ini	sym	prop
full	1.17	0.64	1.47	0.86	0.48
partial	1.26	0.60	0.97	0.79	0.50
patient	1.72	0.58	1.17	1.01	0.61

used to measure the identification error. This error measurement is consistent with the medical definition of the planes.

Figure 5.3 and Table 5.1 show the results of the applied methods on target skulls. These results show that the proposed method can identify FP and MSP accurately and robustly. For FP identification, the proposed automatic method gives an error around 0.61 mm for all the three test cases, which is highly accurate compared to the CT resolution (0.47 to 1 mm/pixel).

For MSP identification, the proposed method is also very accurate. It identified MSPs closer to the midline landmarks than did the symmetry-based method. The error of the proposed method is consistently lower than that of the symmetry-based method for all test cases.

In addition, the proposed method is robust to the asymmetry in skulls. Its accuracy on full and partial skulls are roughly the same (0.48 mm and 0.50 mm) because important landmark points can be located on them. The small increase in error for patient skulls is within an acceptable range because patient skulls have fractures.

In contrast, test results show that the symmetry-based method is less robust because it uses all the mesh vertices, most of which are outliers in defining MSP. Compared to partial skulls, full skulls have top and bottom parts, which tend to be outliers. Therefore, the symmetry-based method, using all the mesh vertices, has a larger error on full skulls. Patient skulls have more outliers than partial skulls due to fractures. Therefore, the error for patient skulls is the largest.

Overall, the proposed method is consistently accurate in identifying both FP, MSP and midline landmarks on all kinds of skulls. Moreover, in identifying MSP, the proposed method, using only the midline features, is more accurate and robust than the symmetry-based method.

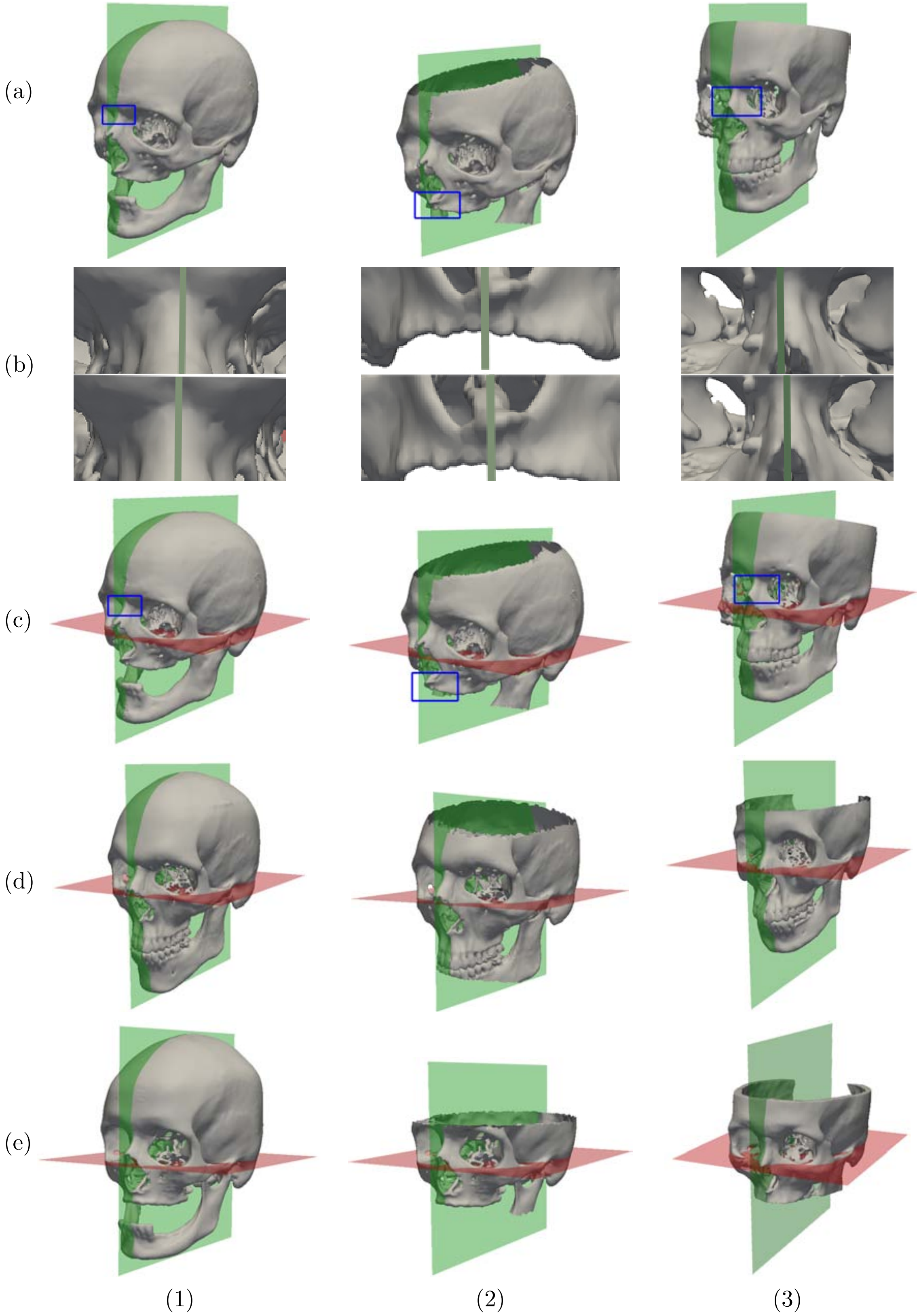

Figure 5.3: Identified MSP and FP. (1) Full skulls. (2) Partial skulls of (1). (3) Patient Skulls. (a) MSP of the models in (c) detected by symmetry-based method. (b) Zoom-in comparison of (a) on top and (c) at bottom. (c–e) Planes detected by proposed method.

Chapter 6

Conclusion

Chapter 1 of this proposal introduced the research problem and presented the research goal by introducing the necessaries of pre-operative planning of CMF surgery and the lack of a predictive system that can assist the surgeon easily perform the planning. Chapter 2 provided the medical knowledge on the skull anatomy, skull deformities, and CMF surgery that serve as the background of this research. Chapter 3 reviewed the state-of-the-arts in the related research field on skull restoration, skull reconstruction, and surgical simulation systems. The limitations of them were also analyzed and presented in Chapter 3. Following, in Chapter 4, the proposed procedure and the core algorithm were presented. Chapter 5 showed the preliminary work.

This thesis proposal developed a computer-aided procedure for the pre-operative planning of craniomaxillofacial (CMF) surgeries. This procedure, first segments the patient's bone fragment from medical images and constructs his/her deformed model from the segmentation result, then acquires surgical requirements from the surgeon through a graphical user interface, and finally restores the patient's skull model based on the requirements.

Surgical requirements of the restoration method are analyzed from the surgeon's perspective. They are: (1) no collision, (2) symmetry, (3) midline, (4) normality and (5) joint continuity. These requirements are translated to four principles that guide the restoration algorithm: (1) symmetry principle, (2) midline principle, (3) normality principle and (4) ordering principle. The restoration algorithm is designed based on the four principles. It orders the movable bone fragments using ordering principle and repositions each of them using the symmetry, midline and normality principle.

A list of research tasks that are involved in the completing the proposed research are identified. Preliminary works have accomplished some of them. For the remaining ones, a detailed schedule is provided.

One contribution of the proposed work is that it provides a tool for easy CMF surgery planning. When applied in real surgical applications, it would greatly improve the effectiveness and accuracy of the CMF surgery planning. Another contribution is that the proposed restoration method can be easily extended for restoration of other fractured rigid objects such as potteries, chinaware and skulls in archeology.

References

[AAG09] Anderson D., Anderson L., Glanze W.: *Mosby's Medical Dictionary.* Mosby St. Louis, 2009.

[AGG*03a] Agus M., Giachetti A., Gobbetti E., Zanetti G., Zorcolo A.: Adaptive techniques for real-time haptic and visual simulation of bone dissection. In *Virtual Reality, 2003. Proceedings. IEEE* (2003), IEEE, pp. 102–109.

[AGG*03b] Agus M., Giachetti A., Gobbetti E., Zanetti G., Zorcolo A.: Real-time haptic and visual simulation of bone dissection. *Presence: Teleoperators & Virtual Environments 12*, 1 (2003), 110–122.

[AGG*04] Agus M., Giachetti A., Gobbetti E., Zanetti G., Zorcolo A.: Hardware-accelerated dynamic volume rendering for real-time surgical simulation. In *Workshop on Virtual Reality Interactions and Physical Simulations* (2004), Citeseer, pp. 20–21.

[BCT*04] Bhandarkar S., Chowdhury A., Tang Y., Yu J., Tolllner E.: Surface matching algorithms computer aided reconstructive plastic surgery. In *Proc. of IEEE Int. Symp. on Biomedical Imaging: From Nano to Macro* (2004), pp. 740–743.

[BM92] Besl P., McKay N.: A Method for Registration of 3D Shapes. *IEEE Trans. on Pattern Analysis and Machine Intelligence 14*, 2 (1992), 239–256.

[BPM*00] Bettega G., Payan Y., Mollard B., Boyer A., Raphaël B., Lavallee S.: A simulator for maxillofacial surgery integrating 3d cephalometry and orthodontia. *Computer Aided Surgery 5*, 3 (2000), 156–165.

[BSMG09] Benazzi S., Stansfield E., Milani C., Gruppioni G.: Geometric morphometric methods for three-dimensional virtual reconstruction of a fragmented cranium: the case of Angelo Poliziano. *International journal of legal medicine 123*, 4 (2009), 333–344.

[CBRY06] Chowdhury A., Bhandarkar S., Robinson R., Yu J.: Virtual craniofacial reconstruction from computed tomography image sequences exhibiting multiple fractures. In *Proc. of IEEE Int Conf. on Image Processing* (2006), pp. 1173–1176.

[CBRY07] Chowdhury A., Bhandarkar S., Robinson R., Yu J.: Novel graph theoretic enhancements to ICP-based virtual craniofacial reconstruction. In *Proc. of IEEE Int. Symp. on Biomedical Imaging: From Nano to Macro* (2007), pp. 1136–1139.

[CHV99] Cavalcanti M., Haller J., Vannier M.: Three-Dimensional Computed Tomography Landmark Measurement in Craniofacial Surgical Planning: Experimental Validation in Vitro. *J. Oral and Maxillofacial Surgery 57*, 6 (1999), 690–694.

[CLL11] Cheng Y., Leow W. K., Lim T. C.: Automatic Identification of Frankfurt Plane and Mid-Sagittal Plane of Skull. In *WACV 2011: IEEE International Workshop on Applications of Computer Vision* (2011), pp. 233–238.

[CMC*04] Chabanas M., Marecaux C., Chouly F., Boutault F., Payan Y.: Evaluating soft tissue simulation in maxillofacial surgery using preoperative and postoperative ct scans. In *CARS* (2004).

[CMPB02] Chabanas M., Marecaux C., Payan Y., Boutault F.: Models for planning and simulation in computer assisted orthognatic surgery. In *MICCAI '02: Proceedings of the 5th International Conference on Medical Image Computing and Computer-Assisted Intervention* (2002), pp. 315–322.

[CP00] Chabanas M., Payan Y.: A 3D Finite Element model of the face for simulation in plastic and maxillo-facial surgery. In *MICCAI '00: Proceedings of the rd International Conference on Medical Image Computing and Computer-Assisted Intervention* (2000), Springer, pp. 411–496.

[CSP*07] Chapuis J., Schramm A., Pappas I., Hallermann W., Schwenzer-Zimmerer K., Langlotz F., Caversaccio M.: A new system for computer-aided preoperative planning and intraoperative navigation during corrective jaw surgery. *Information Technology in Biomedicine, IEEE Transactions on 11*, 3 (2007), 274–287.

[CTS*10] Cevidanes L., Tucker S., Styner M., Kim H., amd Mauricio Reyes J. C., Proffit W., Turvey T., , Jaskolka M.: 3D Surgical Simulation. *Am J Orthod Dentofacial Orthop 138*, 3 (2010), 361–371.

[DGL*01] Dutreuil J., Goulette F., Laurgeau C., Zoreda J. C., Lundgren S.: Computer assisted dental implantology: A new method and a clinical validation. In *MICCAI '01: Proceedings of the 4th International Conference on Medical Image Computing and Computer-Assisted Intervention* (2001), pp. 384–391.

[DMCP*06] De Momi E., Chapuis J., Pappas I., Ferrigno G., Hallermann W., Schramm A., Caversaccio M.: Automatic extraction of the mid-facial plane for cranio-maxillofacial surgery planning. *International journal of oral and maxillofacial surgery 35*, 7 (2006), 636–642.

[Edm65] Edmonds J.: Paths, trees, and flowers. *Canadian Journal of mathematics 17*, 3 (1965), 449–467.

[GEH*99] Glombitza G., Evers H., Hassfeld S., Engelmann U., Meinzer H.: Virtual surgery in a tele-radiology framework. *Information Technology in Biomedicine, IEEE Transactions on 3*, 3 (1999), 186–196.

[GIR04] Gladilin E., Ivanov A., Roginsky V.: Generic approach for biomechanical simulation of typical boundary value problems in cranio-maxillofacial surgery planning. In *MICCAI '04: Proceedings of the 7th International Conference on Medical Image Computing and Computer-Assisted Intervention* (2004), Springer, pp. 380–388.

[Gmb] GmbH V. I.: Amira. [Online; accessed 29-Feb-2012].

[GMBW04] Gunz P., Mitteroecker P., Bookstein F., Weber G.: Computer aided reconstruction of human crania. *BAR International Series 1227* (2004), 92–95.

[GTH*03] Gassner R., Tuli T., Hächl O., Rudisch A., Ulmer H.: Cranio-maxillofacial trauma: a 10 year review of 9543 cases with 21 067 injuries. *Journal of Cranio-Maxillofacial Surgery 31*, 1 (2003), 51–61.

[GWL99a] Gumprecht H., Widenka D., Lumenta C.: Brainlab vectorvision neuronavigation system: technology and clinical experiences in 131 cases. *Neurosurgery 44*, 1 (1999), 97.

[GWL99b] Gumprecht H., Widenka D., Lumenta C.: BrainLab VectorVision Neuronavigation System: technology and clinical experiences in 131 cases. *Neurosurgery 44*, 1 (1999), 97.

[GZDH01] Gladilin E., Zachow S., Deuflhar P., Hege H.: Validation of a linear elastic model for soft tissue simulation in craniofacial surgery. In *SPIE Medical Imaging Conference* (2001).

[GZDH03] Gladilin E., Zachow S., Deuflhard P., Hege H.: Realistic prediction of individual facial emotion expressions for craniofacial surgery simulations. In *Visualizatoin, Image-Guided Procedures, and Display* (2003).

[Har97] Hartley R.: In defense of the eight-point algorithm. *Pattern Analysis and Machine Intelligence, IEEE Transactions on 19*, 6 (1997), 580–593.

[JKS95] Jain R., Kasturi R., Schunck B.: *Machine vision*, vol. 5. McGraw-Hill New York, 1995.

[KGA*96] Keeve E., Girod S., Augustin A., Binner A., Girod B.: Interactive craniofacial surgery simulation. In *ACM SIGGRAPH* (1996).

[KGPG96] Keeve E., Girod S., Pfeifle P., Girod B.: Anatomy-based facial tissue modeling using the finite element method. In *IEEE Visualization* (1996).

[KGRG98] Keeve E., Girod S., R.Kikinis, Girod B.: Deformable modeling of facial tissue for craniofacial surgery simulation. *Computer Aided Surgery* (1998).

[KRG*99] Koch R., Roth S., Gross M., Zimmermann A., Sailer H.: A framework for facial surgery simulation. In *Spring Conference on Computer Graphics* (1999).

[KSS09] Kerwin T., Shen H.-W., Stredney D.: Enhancing realism of wet surfaces in temporal bone surgical simulation. *IEEE Transactions on Visualization and Computer Graphics 15*, 5 (2009), 747–758.

[KWT88] Kass M., Witkin A., Terzopoulos D.: Snakes: Active contour models. *International journal of computer vision 1*, 4 (1988), 321–331.

[LAV09] Lüthi M., Albrecht T., Vetter T.: Building shape models from lousy data. *Medical Image Computing and Computer-Assisted Intervention–MICCAI 2009* (2009), 1–8.

[LC87] Lorensen W., Cline H.: Marching cubes: A high resolution 3d surface construction algorithm. In *ACM Siggraph Computer Graphics* (1987), vol. 21, ACM, pp. 163–169.

[LCL*02] Lee M., Chang C., Lin C., Lo L., Chen Y.: Custom implant design for patients with cranial defects. *Engineering in Medicine and Biology Magazine, IEEE 21*, 2 (2002), 38–44.

[LCL*03] Lee M., Chang C., Lin C., Lo L., Chen Y.: T medical rapid prototyping in custom implant design for craniofacial reconstruction. In *Systems, Man and Cybernetics, 2003. IEEE International Conference on* (2003), vol. 3, IEEE, pp. 2903–2908.

[Lit10] LittleBabyFaceFoundation: Facial deformities. http://www.littlebabyface.org, 2010.

[LP98] Langdon J., Patel M.: *Operative maxillofacial surgery.* Chapman & Hall Medical, 1998.

[Ltd06] Ltd I.: *Patient Information Guide to Inion CMF (Craniomaxillofacial) Surgery.* Inion Ltd, 2006.

[Mim] Mimics M.: Materialise surgicase cmf. [Online; accessed 19-Jan-2011].

[MRR*53] Metropolis N., Rosenbluth A., Rosenbluth M., Teller A., Teller E.: Equation of state calculations by fast computing machines. *The journal of chemical physics 21* (1953), 1087.

[MSB*06] Morris D., Sewell C., Barbagli F., Salisbury K., Blevins N., Girod S.: Visuohaptic simulation of bone surgery for training and evaluation. *Computer Graphics and Applications, IEEE 26*, 6 (2006), 48–57.

[MSCP04] Mollemans W., Schutyser F., Cleynenbreugel J., P.Suetens: Fast soft tissue deformation with tetrahedral mass spring model for maxillofacial surgery planning systems. In *MICCAI '04: Proceedings of the 7th International Conference on Medical Image Computing and Computer-Assisted Intervention* (2004), Springer, pp. 371–379.

[MSCS03] Mollemans W., Schutyse F., Cleynenbreugel J., Suetens P.: Tetrahedral mass spring model for fast soft tissue deformation. In *Lecture Notes in Computer Science* (2003).

[Phi05] Philip G.: *Statistical and geometric reconstruction of hominid crania: reconstructing australopithecine ontogeny.* PhD thesis, University of Vienna, Austria, 2005.

[PLT07] Phillips J. M., Liu R., Tomasi C.: Outlier robust ICP for minimizing fractional RMSD. In *Proc. of Int. Conf. on 3D Digital Imaging and Modeling* (2007), pp. 427–434.

[RRS03] Rossi M., Ribeiro E., Smith R.: Craniofacial asymmetry in development: an anatomical study. *The Angle orthodontist 73*, 4 (2003), 381.

[SBF*04] Schmidt J. G., Berti G., Fingberg J., Cao J., Wollny G.: A finite element based tool chain for the planning and simulation of maxillo-facial surgery. In *ECCOMAS 2004: European Congress on Computational Methods in Applied Science and Engineering* (2004).

[SH] Siwek D., Hoyt R.: Anatomy of the human skull. `http://skullanatomy.info`.

[SS04] Sezgin M., Sankur B.: Survey over image thresholding techniques and quantitative performance evaluation. *Journal of Electronic imaging 13* (2004), 146.

[SVBBC09] San Vicente G., Buchart C., Borro D., Celigueta J.: Maxillofacial surgery simulation using a mass-spring model derived from continuum and the scaled displacement method. *International journal of computer assisted radiology and surgery 4*, 1 (2009), 89–98.

[Tay01] Taylor K.: *Forensic art and illustration.* CRC, 2001.

[TGG99] Teschner M., Girod S., Girod B.: Optimization approaches for soft-tissue prediction in craniofacial surgery simulation. In *MICCAI '99: Proceedings of the 2nd International Conference on Medical Image Computing and Computer-Assisted Intervention* (1999), Springer, pp. 1183–1190.

[TPS*02] Troulis M., P.Everett, Seldin E., Kikinis R., Kaban L.: Development of a three-dimesional treatment planning system based on computed tomographic data. *Journal of Oral Maxillofacial Surgery* (2002).

[TVE*07] Tardieu P., Vrielinck L., Escolano E., Henne M., Tardieu A.-L.: Computer-assisted implant placement: scan template, SimPlant, SurgiGuide, and SAFE system. *The International Journal of Periodontics & Restorative Dentistry 27*, 2 (2007), 141–149.

[VvCM*96] Verstreken K., van Cleynenbreugel J., Marchal G., van Steenberghe D., Suetens P.: Computer-assisted planning of oral implant surgery - an approach using virtual reality. In *Proceedings of the 4th Medicine Meets Virtual Reality* (1996), pp. 423–434.

[Wik09] Wikipedia: Human skull, 2009. `http://en.wikipedia.org/wiki/Human_skull`,.

[Wik10] Wikipedia: Cleft lip and palate, 2010. [Online; accessed 10-Jan-2010].

[Wik12] Wikipedia: Traffic collision, 2012. [Online; accessed 27-Feb-2012].

[Woo31] Woo T.: On the asymmetry of the human skull. *Biometrika 22*, 3/4 (1931), 324–352.

[Wro10] WrongDiagnosis: statistics by country for cleft palate. http://WrongDiagnosis.com/, 2010.

[WYLL11] Wei L., Yu W., Li M., Li X.: Skull assembly and completion using template-based surface matching. In *3D Imaging, Modeling, Processing, Visualization and Transmission (3DIMPVT), 2011 International Conference on* (2011), IEEE, pp. 413–420.

[XGT05] Xia J., Gateno J., Teichgraeber J. F.: Three-dimensional computer-aided surgical simulation for maxillofacial surgery. In *Atlas of the Oral and Maxillofacial Surgery Clinics* (2005), pp. 25–39.

[XIS*00] Xia J., Ip H., Samman N., Wang D., Kot C., Yeung R., Tideman H.: Computer-assisted three-dimensional surgical planning and simulation: 3D virtual osteotomy. *International journal of oral and maxillofacial surgery 29*, 1 (2000), 11–17.

[XSC*00] Xia J., Samman N., Chua C. K., Yeung R. W. K., Wang D., Shen S. G., Ip H. H.-S., Tideman H.: PC-based virtual reality surgical simulation for orthognathic surgery. In *MICCAI '00: Proceedings of the 3th International Conference on Medical Image Computing and Computer-Assisted Intervention* (2000), pp. 1019–1028.

[YPH*06] Yushkevich P., Piven J., Hazlett H., Smith R., Ho S., Gee J., Gerig G.: User-guided 3d active contour segmentation of anatomical structures: significantly improved efficiency and reliability. *Neuroimage 31*, 3 (2006), 1116–1128.

[ZGSZ03] Zachow S., Gladilin E., Sader R., Zeilhofer H.: Draw and cut: intuitive 3d osteotomy planning on polygonal bone models. In *International Congress Series* (2003), vol. 1256, Elsevier, pp. 362–369.

[ZLES05] Zachow S., Lamecker H., Elsholtz B., Stiller M.: Reconstruction of mandibular dysplasia using a statistical 3D shape model. In *International Congress Series* (2005), vol. 1281, Elsevier, pp. 1238–1243.